Premature capacity (PCL) loss in Lead Acid batteries

Shedding and aging of the PbO_2 electrode

A research program carried out
at Battelle Geneva Switzerland
from 4/1977 to 4/1978

Part 2 from page 56

By
H.Giess
M.M Janssoone

This general tendency of low reactivity coupled with improved particle-to-particle welding would explain the improved performances of the Sb grid electrodes, although the direct link still remains to be precisely determined.

3.5. THE EFFECTS OF ANTIMONY ON THE CYCLING BEHAVIOUR OF THE POSITIVE ELECTRODE

The following chapters will present in detail the different positive effects of antimony on the cycle life of the positive electrode. A résumé of these effects and their appearance is shown in Fig. 79.

The LODEF effect is assimilated to the Sb^{III} effect.

3.5.1. THE ANTIMONY 1 EFFECT

The Sb^{I} effect observed in our comparative investigation concerns the apparent better active mass utilization observed from the 1st cycle till E.O.L. when antimony is present in the grid, or introduced (i) artificially as a Sb-coating on the grid or (ii) as Sb metal powder mixed into the reacted paste. A typical example of such active mass utilization differences is shown in Fig. 80.

This behaviour was systematically observed in all our electrode preparation sets.

Table 21 shows the differences in $Ah \cdot g^{-1}$ of identical electrodes which referred to the equivalent 7 Sb or 5 Sb electrode, arbitrarly set at 1.000.

56 a

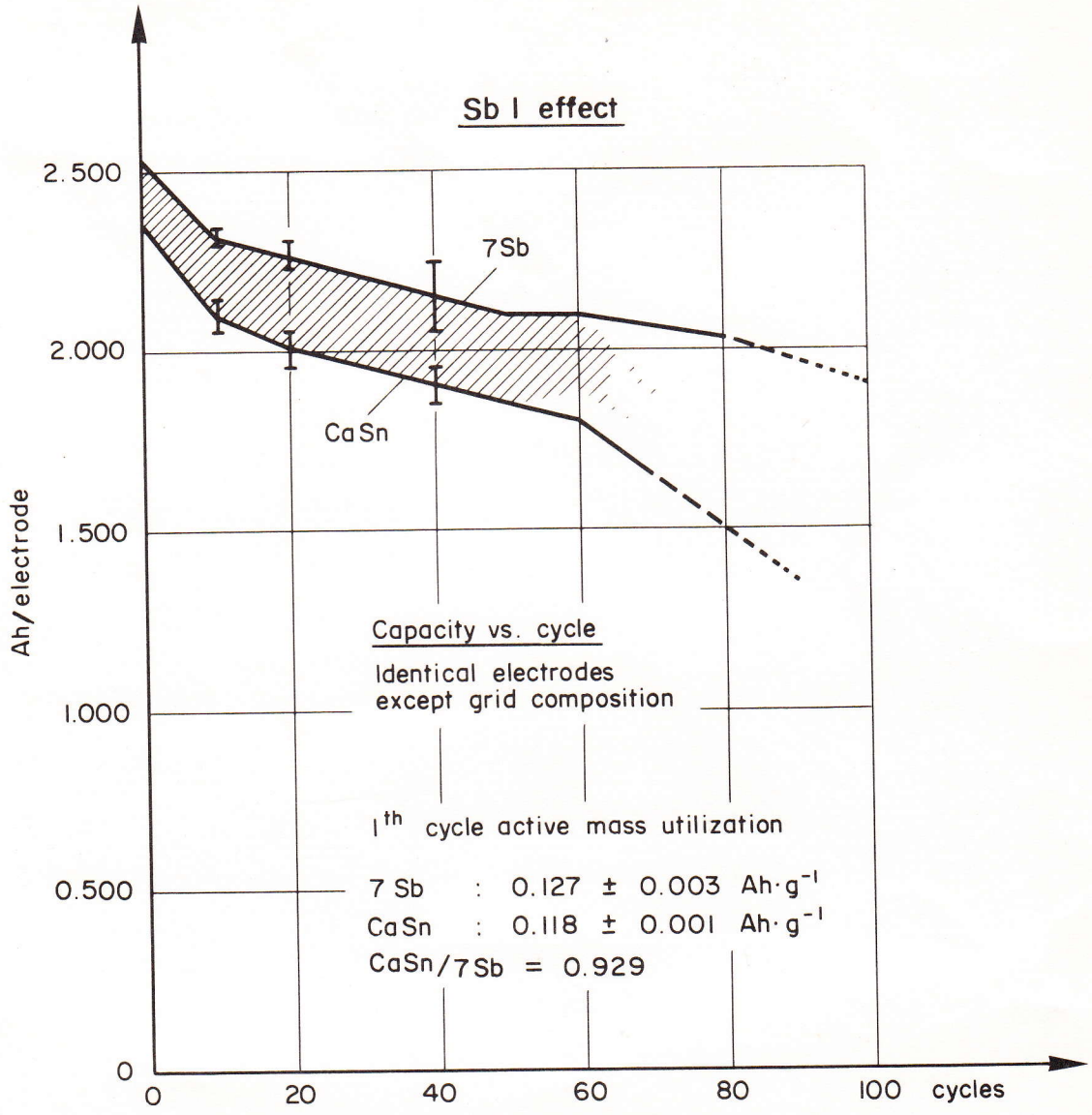

Fig. 80 The Sb^{I} effect.
Improved active mass utilization in presence of antimony.

TABLE 21

TEST a	7 Sb = 1.000	(actual value 1.260 $\pm$ 0.001 (*) $Ah \cdot g^{-1}$)
	4.5 Sb = 0.968	(0.122 $\pm$ 0.004 $Ah \cdot g^{-1}$)
	2.7 Sb = 0.960	(0.121 $\pm$ 0.004 $Ah \cdot g^{-1}$)
	CaSn = 0.937	(0.118 $\pm$ 0.002 $Ah \cdot g^{-1}$)
TEST b	7 Sb = 1.000	(0.127 $\pm$ 0.001 $Ah \cdot g^{-1}$)
	4.5 Sb = 0.976	(0.124 $\pm$ 0.002 $Ah \cdot g^{-1}$)
	2.7 Sb = 0.969	(0.123 $\pm$ 0.002 $Ah \cdot g^{-1}$)
	CaSn = 0.929	(0.118 $\pm$ 0.002 $Ah \cdot g^{-1}$)
TEST c	5 Sb = 1.000	(0.131 + 0.002 $Ah \cdot g^{-1}$)
	3.3 Sb = 0.977	(0.128 $\pm$ 0.001 $Ah \cdot g^{-1}$)
	CaSn = 0.924	(0.121 $\pm$ 0.002 $Ah \cdot g^{-1}$)
	CdSb = 0.931	(0.122 $\pm$ 0.002 $Ah \cdot g^{-1}$) N.B. slightly different grid and 1.33% Sb

(*) standard deviation

From these excerpts of available data it is apparent that the active mass utilization is related to the presence of antimony in the grid. With Sb-free grids, electrodes show,with all other factors constant, between 6 to 7% less specific capacity when tested under strictly comparative discharge conditions of a ~ 3.5 hour rate to a fixed positive electrode potential of +500 mV vs Hg/Hg_2SO_4. Not only was the presence or absence of Sb felt, but also its relative amount present in the grid. The effect of improved active mass utilization in the presence of increasing amounts of antimony is visible from Fig. 81 where the relative analytically determined Sb concen-

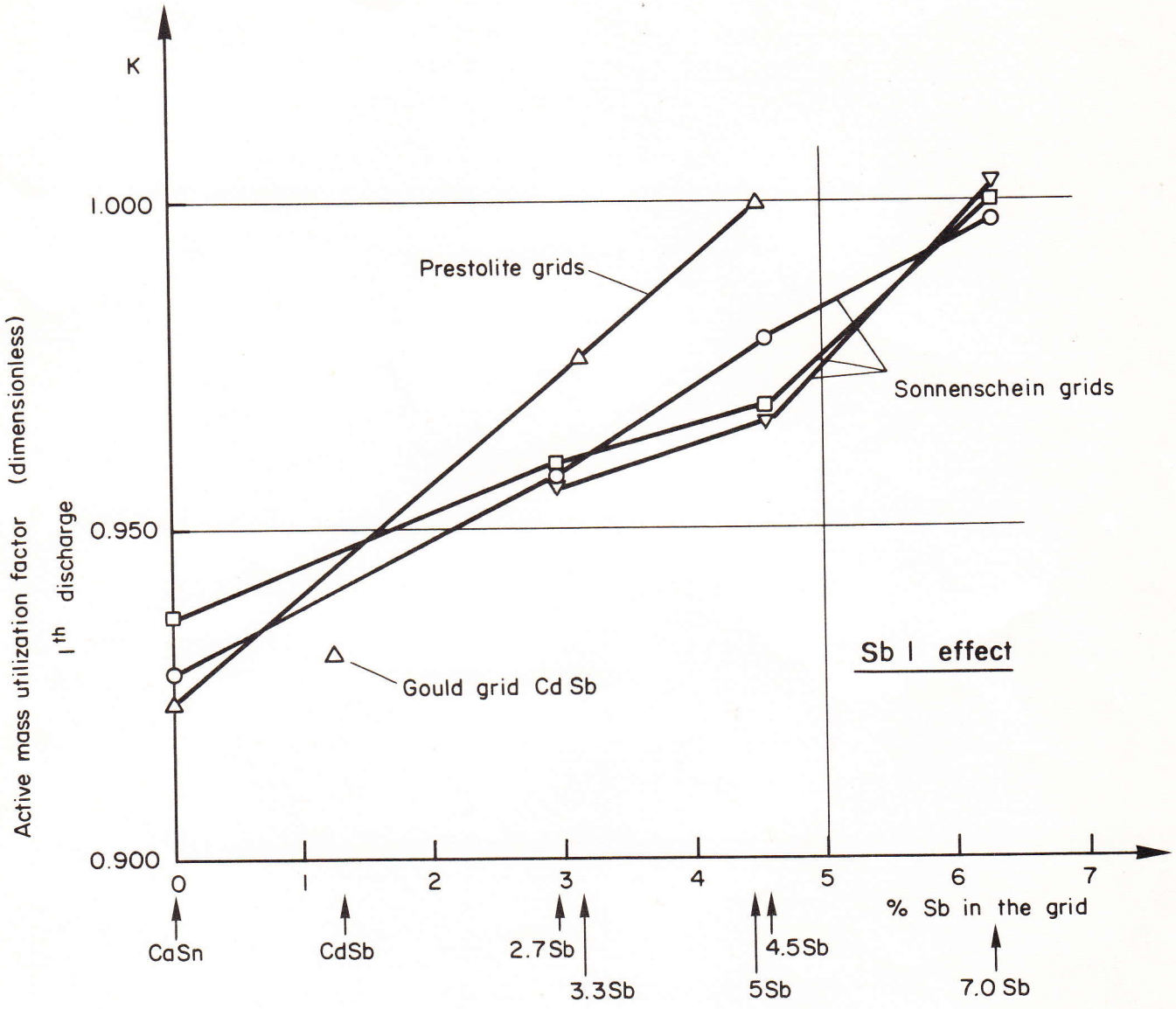

Fig. 81 Active mass utilization vs Sb concentration in the grid.

tration in the grid is related to the dimensionless factor K of active mass utilization at the first discharge. These active mass utilization factors decrease as a function of the cycle life of the electrode, but the sequence 7 Sb > 4.5 Sb > 2.7 Sb > CaSn is maintained through life.

The electrodes prepared by DELCO-GM showed a more ambiguous behaviour as shown below in Table 22, Set 1, 2, 3.

TABLE 22

TEST	K	$Ah \cdot g^{-1}$	NOTE
SET 1			
7 Sb	1.000	0.095 ± 0.004	Reference DELCO-2
CaSn	0.916	0.087 ± 0.002	DELCO-2 - no shrinkage fractures
7 Sb	1.000	0.076 ± 0.002	Reference DELCO-1
CaSn	0.895	0.068 ± 0.001	DELCO 1 - no shrinkage fractures
SET 2			
7 Sb	1.000	0.088 ± 0.001	DELCO-2 formed to 0.74 $Ah \cdot g^{-1}$
CaSn	1.023	0.090 ± 0.004	DELCO-2 formed to 0.74 $Ah \cdot g^{-1}$
7 Sb	1.000	0.088 ± 0.001	DELCO-2 formed to 0.74 $Ah \cdot g^{-1}$
CaSn	1.011	0.089 ± 0.001	DELCO-2 formed to 0.74 $Ah \cdot g^{-1}$
SET 3			
7 Sb	1.000	0.089 ± 0.005	DELCO-3 formed to 0.56 $Ah \cdot g^{-1}$
4.5 Sb	1.079	0.096 ± 0.001	DELCO-3 formed to 0.56 $Ah \cdot g^{-1}$
2.7 Sb	1.002	0.091 ± 0.004	DELCO-3 formed to 0.56 $Ah \cdot g^{-1}$
CaSn	1.034	0.092 ± 0.002	DELCO-3 formed to 0.56 $Ah \cdot g^{-1}$
7 Sb	1.000	0.089 ± 0.003	DELCO-3 formed to 0.56 $Ah \cdot g^{-1}$
4.5 Sb	1.056	0.094 ± 0.001	DELCO-3 formed to 0.56 $Ah \cdot g^{-1}$
2.7 Sb	1.067	0.095 ± 0.001	DELCO-3 formed to 0.56 $Ah \cdot g^{-1}$
CaSn	1.045	0.093 ± 0.002	DELCO-3 formed to 0.56 $Ah \cdot g^{-1}$

The confirmation of the Sb-content/specific active mass utilization correlation has therefore also been sought with electrodes where the Sb and Sb-relatable factors were artificially changed. These tests consisted in

(a) adding antimony (metal) in the interface grid-active mass of CaSn electrodes;

(b) adding antimony (metal) in the active mass, thus also in the interface of CaSn electrodes;

(c) introducing an inert coating of gold (40 µm Au electroplated) between the lead alloy grid, i.e. 7 Sb or CaSn, and the active mass;

(d) dissolving the available surface antimony from 5 Sb grids through an anodization in 1.06 sp.gr. H_2SO_4 (saturated in Sb_2O_3) for 20 h at 40°C and with 417 mA·electrode^{-1}. This also produces an intermediary PbO_2 layer;

(e) artificially introducing strong shrinkage fractures in the active mass-grid interface of both 7 Sb and CaSn grid electrodes by flash-drying after pasting.

These electrodes, representative of various stages of interface conditions, were formed as described and then discharged. The relative capacity was recorded and the utilization factor K calculated relative to 7% or 5% Sb grid electrodes.

The results are shown in Table 23, Sets 1, 2 and 3.

TABLE 23

TEST	K	$Ah \cdot g^{-1}$	NOTE
SET 1 (in decreasing order)			
CaSn-Sb in AM	1.041	0.128 ± 0.003	0.2% w/w Sb metal powder mixed into the reacted paste
CaSn-Sn in AM	1.008	0.124 ± 0.007	0.2% w/w Sn metal powder mixed into the reacted paste
7 Sb	1.000	0.123 ± 0.004	Reference
CaSn-Sb coating	0.967	0.119 ± 0.003	1.5 µm Sb coating on the grid
CaSn-PbSb in AM	0.951	0.117 ± 0.004	0.2% w/w Sb added to the reacted paste as Pb2%Sb alloy powder
CaSn	0.935	0.115 ± 0.002	Normal CaSn
7 Sb-Au coating	0.927	0.114 ± 0.003	4 µ Au electroplated (pinholes)
CaSn-Au coating	0.919	0.113 ± 0.001	4 µ Au electroplated (pinholes)
SET 2 (in decreasing order)			
7 Sb	1.000	0.116 ± 0.006	Reference
CaSn	0.966	0.112 ± 0.001	Normal with some shrinkage fractures
7 Sb-cracked	0.948	0.110 ± 0.001	Flash-dried electrodes
CaSn-Au	0.931	0.108 ± 0.001	40 µm Au coating
7 Sb-Au	0.931	0.108 ± 0.001	40 µm Au coating
CaSn-cracked	0.914	0.106 ± 0.001	Flash dried electrodes
7 Sb-Au cracked	0.879	0.102 ± 0.003	40 µm Au + flash drying
CaSn-Au cracked	0.879	0.102 ± 0.003	40 µm Au + flash drying

TEST	K	$Ah \cdot g^{-1}$	NOTE
SET_3 (in decreasing order)			
CaSn-Sb coating	1.038	0.137 ± 0.003	1.5 µm Sb coating on the grid
5 Sb	1.000	0.132 ± 0.004	Reference
5 Sb-anodized	0.977	0.129 ± 0.001	Grid anodized in 1.06 sp.gr. H_2SO_4 sat. with Sb_2O_3
CaSn-anodized	0.939	0.124 ± 0.001	Grid anodized in 1.06 sp.gr. H_2SO_4 sat. with Sb_2O_3
CaSn	0.924	0.122 ± 0.002	Normal CaSn with some shrinkage fractures

The evolution of the available specific capacity data reflects the positive effect of antimony on the active mass utilization under a given discharge regime. The statistical significance of the observed differences is in certain cases limited by the overlapping of the uncertainity, i.e. standard deviation values, but one observes practically always a general trend

low Sb ⟶ low active mass utilization.

In addition to the uncertainity introduced by the DELCO preparations, the conclusions for these experiments are:

- the artificial addition of antimony is effective in raising the active mass utilization

  Sb in AM > Sb coating > PbSb in AM > 7 Sb

  Sn in AM ~ Sb in AM (effect probably due to additional porosity formation);

- either the leaching out of Sb from the surface region or the formation of a PbO_2 film, or both combined as in anodized 5 Sb grids, reduces the specific capacity of the electrode to a certain extent;

- the introduction of flash-drying cracks is reflected in both 7 Sb and CaSn electrodes with an additional 5% loss in the capacity of the electrode (NB: flash drying cracks in CaSn yield, as will be discussed later, a 100% failure rate within 20 cycles);

- the presence of a chemically inert layer, i.e. gold coating, decreases the specific capacity, furthermore obliterating practically all the influences from the nature of the substrate alloy, i.e. 7 Sb or CaSn. Thus, the 40 µm gold coated CaSn and 7 Sb electrodes show identical values, approximately 3% lower than a "normal" CaSn electrode and approximately 7% lower than the 7 Sb reference;

- the combination of an inert 40 µm-Au layer (in terms of impeded Sb release and reaction affinity toward the paste) with flash-drying, i.e. the introduction of large amounts of drying cracks, accentuates the reduction of the specific active mass utilization. The utilization decreased by 12% (referred to 7 Sb). Again, the Au coating cancels the differences of the substrate alloy and both types of electrodes (Au-CaSn and Au-7 Sb) fail within 20 cycles.

As a summary of these experiments, we can conclude that a factor which negatively influences the specific mass utilization is the

absence or limited availability of antimony.

The absence of Sb may be derived:

- from the grid alloy composition (CaSn);
- from surface leaching of antimony (anodization);
- from an inert, Sb impervious coating on the antimonial grid alloy.

Furthermore, the *presence of flash-drying cracks* in the electrodes also contributes to the lower active mass utilization. As will be discussed later, the combined presence of drying cracks and the absence (CaSn) or non-availability (7 Sb + Au) of antimony, results in a drastic capacity loss within 20 cycles.

The observed *antimony = better specific mass capacity* correlation requires a further connection with properties conferred to the positive electrode by the antimony and also a geographic localization of its effect in order to be able to find technological substitutes.

The information available primarily points to the interface region grid-active mass and to the bulk-active mass secondarily as the possible region of such action.

The common denominator of these capacity depressing factors would indicate reduced pathways for electron flow between the active mass and the grid. This would cover:

- reduced adhesion (confirmed);
- shrinkage fractures (confirmed);
- finer PbO_2 crystallites with less particle bond (confirmed);
- incomplete formation of the curing corrosion layer, i.e. ($PbO_{(0)} \rightarrow 4PbO \cdot PbSO_4$) (not thoroughly confirmed).

As the presence of shrinkage fractures was negatively influencing the first cycle capacity, we suggest that by improving the active mass-grid bond, the presence of antimony exercises its influence on the specific active mass utilization.

3.5.2. THE Sb^{II} EFFECT - EARLY FAILURES

Antimony's most critical action on the deep cycling behaviour of positive electrodes resides in the prevention of a drastic capacity loss within 20 deep discharge cycles as experienced in a varying degree with Sb-free electrodes.

This phenomena, called the Sb^{II} effect, exercises a heavy influence on the successful production of maintenance-free traction batteries employing a flat plate design. In fact, whereas the Sb^{I} and Sb^{III} effects can be foreseen and compensated, the occurrence of the Sb^{II} effect appears to be random, but nevertheless dependent on the preparation history of the electrode. This randomness stems from the difficulty of controlling all parameters of the electrode preparation when employing a standard curing technique.

This preparation and cycling history has practically no influence in terms of "early failures" when Sb-containing grids (minimum tested 1.3% Sb) are employed, but it does become the principal factor for a satisfactory cycle life when Sb-free electrodes are involved.

A typical early failure behaviour is shown in Fig. 82 which is characterized by a capacity decay slope of approximately 0.15 Ah $cycle^{-1}$ vs a normal observed value of approximately 0.01 to 0.03 $Ah \cdot cycle^{-1}$. End of life (EOL), arbitrarly set at a 50% loss of the second cycle capacity, occurred between 10 and 20 cycles. This

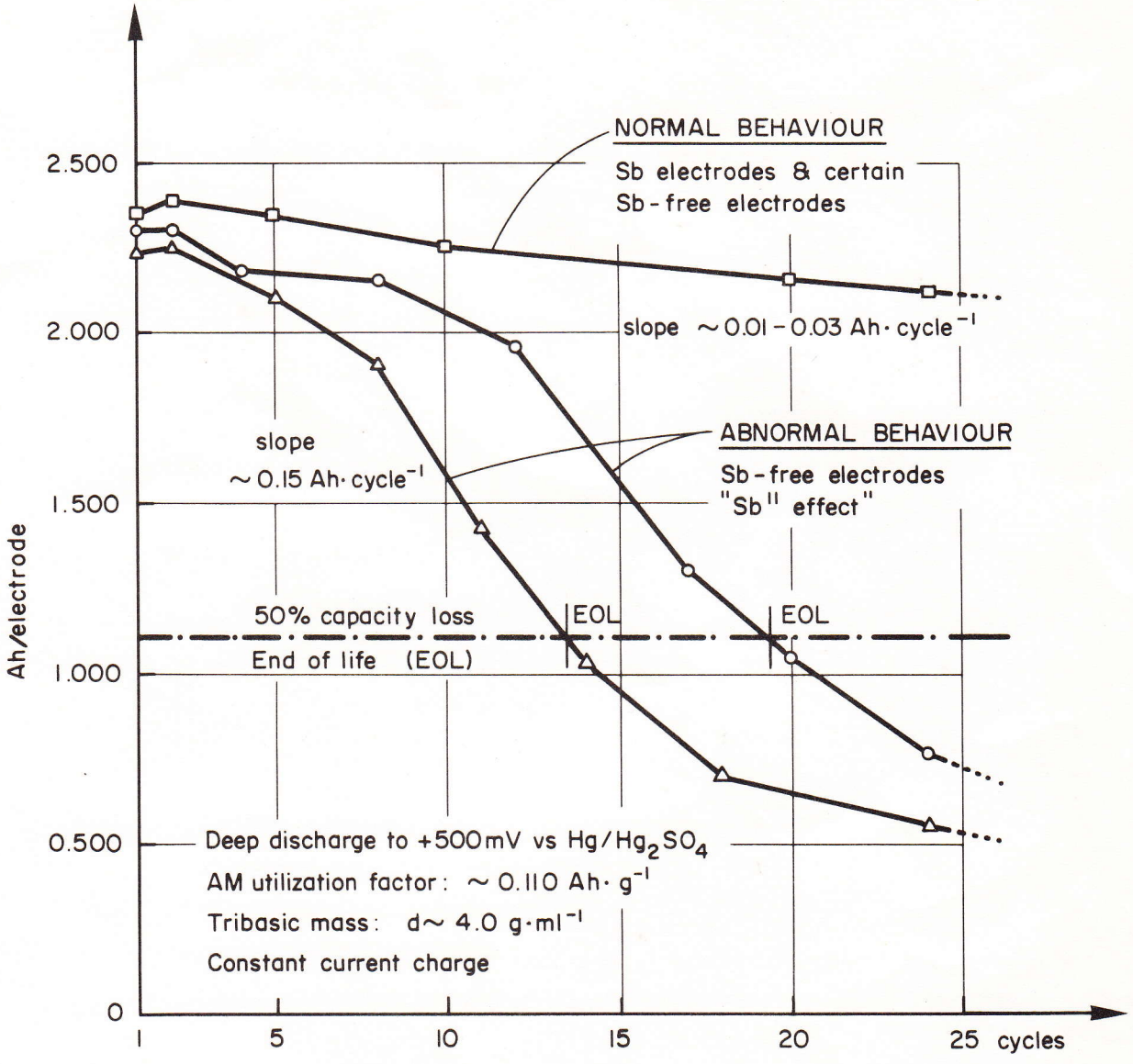

Fig. 82 The Sb^{II} effect.

Early failure of Sb-free electrodes during deep discharge cycling.

failure, which we will now discuss for the standard tribasic paste preparations, was experienced with Battelle-Geneva electrode preparations and with industrially prepared electrodes manufactured by PRESTOLITE and SONNENSCHEIN and therefore represents a real effect. We recall that the set of plates prepared by DELCO did not show these phenomena.

These phenomena are discussed to a certain extent in the pertinent literature and are also the object of an ongoing study financed by ILZRO, but up to now no distinction has been made between the different Sb effects encountered.

The causes of such failures is the object of more or less experimental speculations, such as:

(i) the disintegration of the active mass, i.e. shedding;

(ii) the formation of an isolating film of $PbSO_4$ or PbO;

(iii) the necessity of doping PbO_2 with Sb for satisfactory behaviour;

(iv) the formation of stoichiometric, i.e. isolating PbO_2;

(v) the delamination of the active mass from the grid;

(vi) the formation of dense PbO_2 and related passivation with $PbSO_4$;

(vii) the formation of irreversible "hard" $PbSO_4$ around the grid;

etc., etc.

We therefore had to isolate this effect from the other effects of antimony, which we successfully achieved, and to describe and demonstrate its mechanism and develop efficient and realistic countermeasures on the basis of these data.

The data below will show:

(a) the occurrence of the early failures, and

(b) the results of specific experiments conducted with the purpose of understanding the mechanism.

We recall that the first clues to the failure mode were already obtained by the thorough analysis of the curing related phenomena and by the observed effect of antimony on the crystallization of PbO_2. Furthermore, the fact that a certain amount of electrodes without antimony reached satisfactory cycle lives without showing early failures, led to the conclusion that there is no fundamental barrier in terms of complete incompatibility between the antimony-free conditions and deep cycling, but that the absence of antimony requires a much finer adjustment of the overall preparation and cycling parameters.

Occurrence of the early failure

The occurrence of the early failure was analyzed by simultaneously cycling antimony-containing positive electrodes and antimony-free electrodes from a batch known not to show early failures, and antimony-free electrodes from a batch showing early failures.

The electrodes were cycled in exactly the same previously described way and analyzed in the fully charged or fully discharged status, i.e. the status of the electrode when the positive plate potential reached +500 mV. The amount of $PbSO_4$ in the electrode was

naturally a function of the available capacity at the particular cycle. The discharge current was constant over life which means that fully functional electrodes were discharged at a relative $C_{3.5}$ to $C_{4.5}$ rate, whereas failing electrodes reached the cut-off potential after ~1.0 to 1.5 hours, i.e. the relative rate was much faster ($C_{1.0}$ to $C_{1.5}$).

The selected electrodes were extracted from the test cells, washed for 50 minutes in running deionized water, damp dried with Kleenex tissue paper and dried at 60°C under primary vacuum (~50 Torr).

Portions of electrodes prepared in this way were then embedded by vacuum impregnation in Epoxy and metallographically polished to expose the regions of interest.

The metallographic preparation consisted in:

(a) pregrinding with SiC paper (Nr. 340 - Nr. 600) with water lubrification;

(b) polishing with 1 µm diamond and lapping oil;

(c) ultrasonic cleaning with pentane-trichlorethylene;

(d) final polishing with 0.05 µm γ-Al_2O_3 with water lubrification.

The polishing method and the use of the BUEHLER-MINIMET unit allowed an excellent surface finish to be obtained so that no etching was needed.

We would like to point out that the hardness differences between the base metal-alloying constituents-PbO_2 corrosion layer-PbO_2 active mass, resulted in the formation of reliefs which could

mislead an unexperienced observer when correlating clear or white features with $PbSO_4$. This will be indicated as needed on the images.

The analytical techniques used for this investigation principally employed:

- *optical microscopy with dark-field illumination* as this is the only illumination mode for revealing colour and structure differences and fine details at high magnification;
- *X-ray microprobe analysis* for the detection of sulfur, i.e. lead sulfate.

1) First possible hypothesis for the mechanism of early failures

The active mass disintegrates and sheds massively from the electrode when Sb is absent.

Observable side effects: large quantities of mud, "softness" of the active mass.

This hypothesis is not pertinent as careful analysis of the shedded material quantity revealed no excess of mud and no differentiated softening at this stage of life.

The amount of mud found in the cell at the moment of early failures of Sb-free electrodes (~20 - 24th cycle) is shown in Table 24.

TABLE 24

7 Sb	shedded: 0.260 ± 0.067 g PbO_2	—— 24th cycle	no failure
CaSn	shedded: 0.338 ± 0.091 g PbO_2	—— 24th cycle	no failure
CaSn	shedded: 0.204 g PbO_2	—— 16th cycle	failed

The amount of shedded PbO_2 is thus normal when compared to other experimental sets. In terms of attributable capacity loss (K) calculated according to the formula:

$$K = \frac{\text{g shedded} \times 0.224\ (Ah \cdot g^{-1}) \times 100}{\text{difference in capacity observed (Ah)}} \quad \%$$

the shedded material would cover only 4 to 6% of the capacity loss.

Visual inspection of the grid revealed no gross defects, i.e. no mass pellets missing, nor "buckling" or "softening", thus the phenomena responsible for early failure are different from shedding and softening.

2) Second possible hypothesis for the mechanism of early failures

Fundamental inoperability of the PbO_2 electrode in a deep discharge regime; the PbO_2 "inactivates" without shedding when Sb is not available in the positive electrode.

This hypothesis is not pertinent as the early failures occur in an irregular fashion and parallel experiments with flat and tubular electrodes with non-antimonial grids showed lifetimes comparable to those with antimony available in the system.

Tubular electrodes with a Sn-ASTAG (Sb-free) current collector have now accumulated more than 500 deep discharge cycles (active mass utilization factor ~0.07 $Ah \cdot g^{-1}$ and cumulative life ~33 $Ah \cdot g^{-1}$).

3) Other possible hypotheses for the mechanism of early failures

Defect of the interface.

Now that we have narrowed down the location of the early failure to the next critical region of the positive electrode, i.e. the interface grid-active mass, an entire series of possible scenarios become plausible. To prove and disprove these scenarios, the pertinent investigations are shown in the following pages and figures. We will commence with the description of the phenomena observed.

Evolution of electrode interfaces showing the Sb^{II} effect, i.e. early failure as signaled by a rapid decay of the discharge capacity

Comparative evolution 7 Sb - CaSn

1st stage of evolution:

5 deep discharge cycles.

Capacity: 7 Sb: 2.150 Ah ; CaSn: 2.078 Ah;
CaSn/Sb, 0.97 (relative capacity factor)

Figure 83 (a - b - c - d)

a and b respectively show the low magnification cross-section through the spine and the fully discharged active mass of the 7 Sb and CaSn grid electrode, in addition to the arrows indicating the location of the subsequent magnifications.

c and d outline the interface in greater detail and one can observe the good intergrowth and contact of the discharged active mass with the cycling corrosion layer (CCL) in the antimonial grid electrode, whereas with the antimony-free electrode, the existence of a circumferential fracture between the active mass and CCL is noticeable. This fracture is practically visible on all grid members

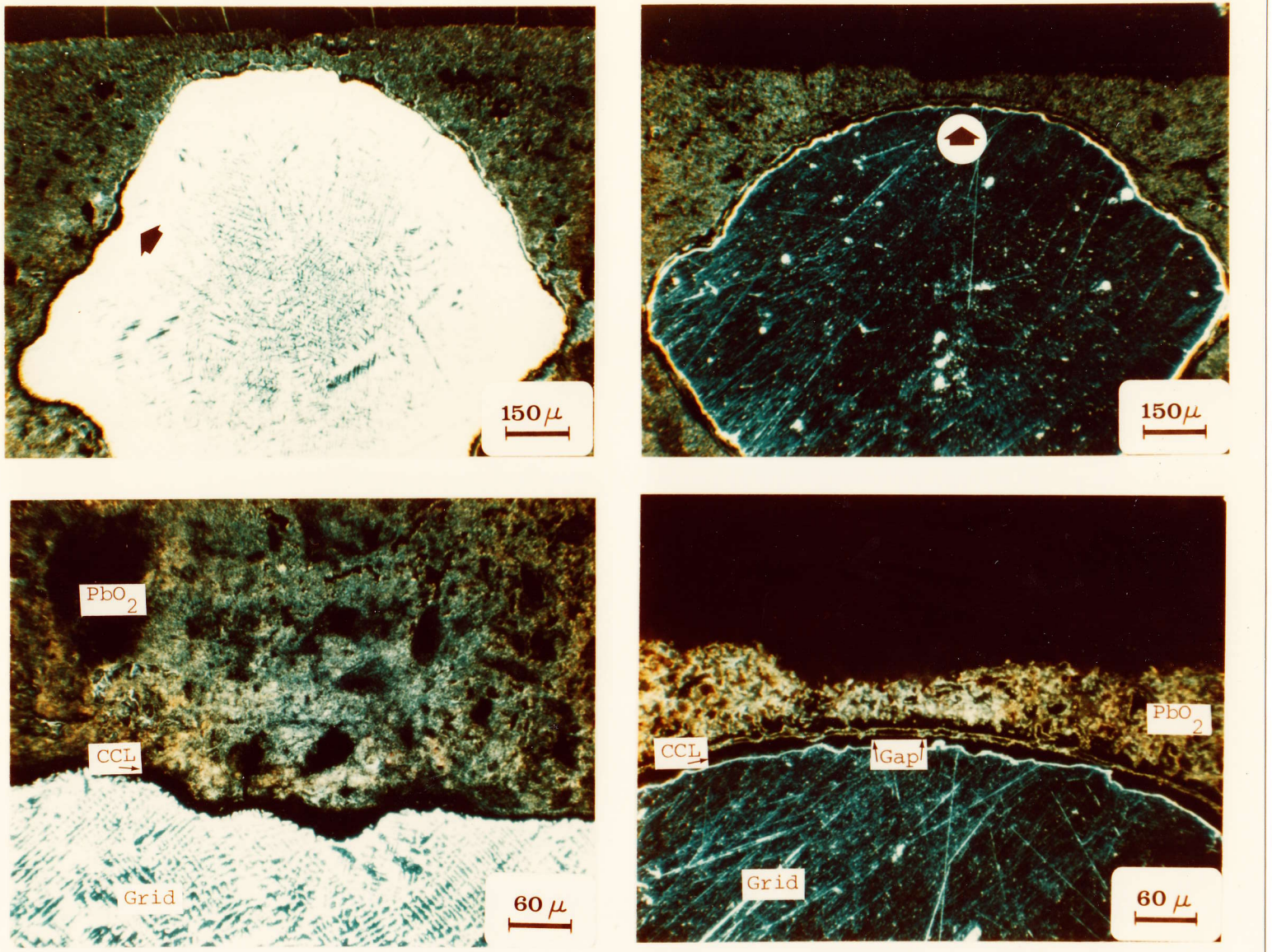

Fig. 83 | a | b | c | d |

1st stage of evolution - 5 discharge cycles - fully discharged status.
a,c 7 Sb electrode - b,d CaSn electrode.

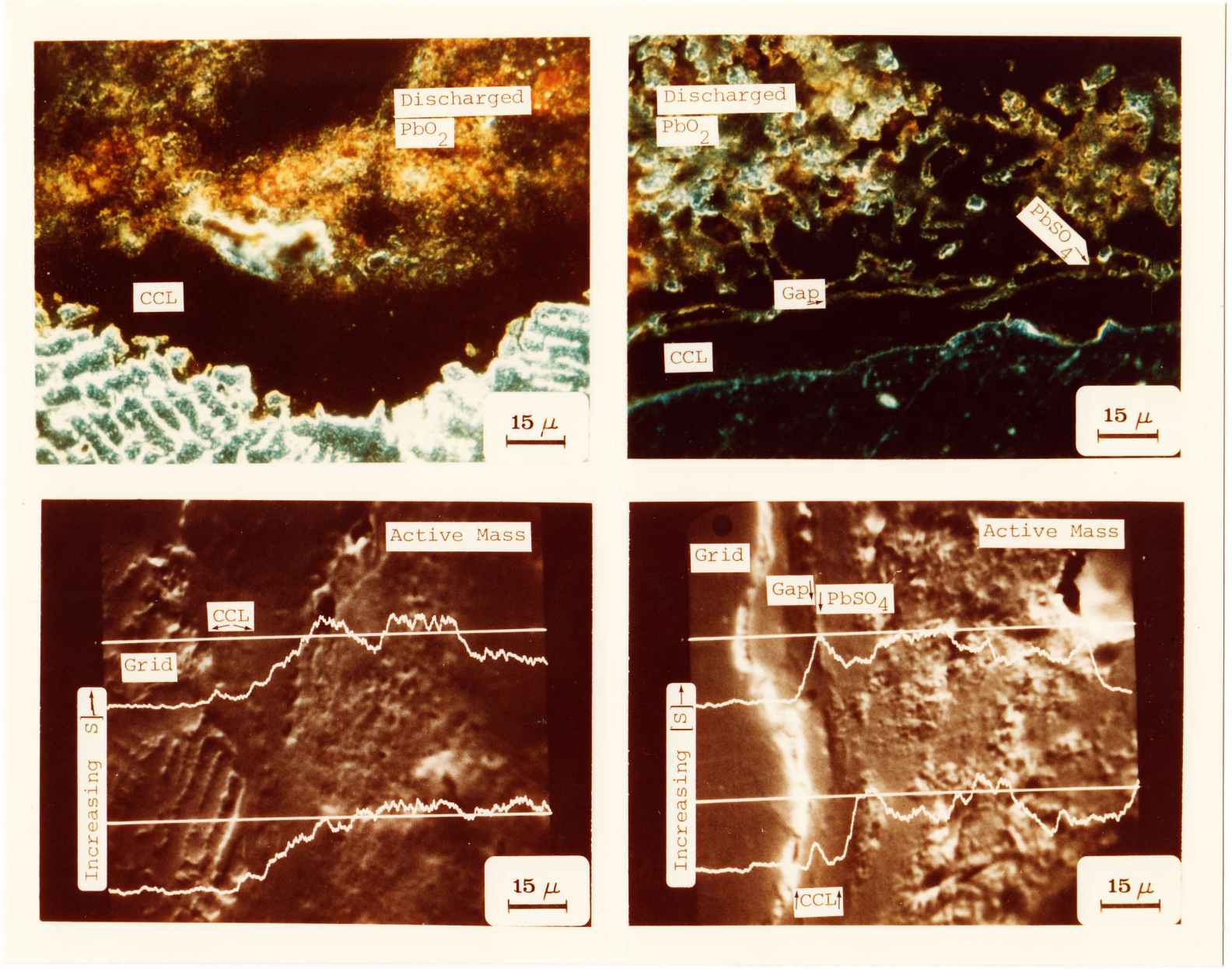

Fig. 84 | a | b | / | c | d | 1st stage of evolution - 5 discharge cycles - fully discharged status.
a,c 7 Sb electrode - b,d CaSn electrode.

and extends through approximately ½ to 2/3 of the interface. In certain locations, this apparent fracture is filled by $PbSO_4$, indicating that a discharge reaction has also occurred in these gaps.

Fig. 84 (a - b - c - d)

a and b show the interface at high magnification with no major physical defects in the 7 Sb electrode,whereas in the CaSn electrode the delamination fracture gave a 3 - 5 µm wide gap between the corrosion layer and the active mass. The internal surface of the gap is covered by lead sulfate. This lead sulfate indicates that H_2SO_4 is available and that bridges existing between the active mass and the CCL are subject to the discharge process, i.e. an attack and disruption of the bridges needed for electronic contact between the active mass and current collector. These bridges are at the moment still partially surviving as indicated by the acceptable electrode capacity. c and d show the X-ray microprobe scans (XRMPS) of sulfur, i.e. $PbSO_4$ superimposed on the SEM image of the respective interfaces.
(The continuous straight white line indicates the precise location of the analysis path, and the irregular line the relative sulfur concentration).

In the interface AM-grid, a monotonous increase of the relative $PbSO_4$ concentration in the CCL is observed with the 7 Sb electrode when we move from the grid-CCL interface toward the CCL-active mass interface.

In d, we observe that the gaps and clear bands noticed in the CCL and CCL-AM interface give a locally stronger sulfur, i.e. $PbSO_4$,signal, confirming the optical observation of local discharge sites. These discharge sites affect the electrode behaviour principally by weakening and destroying the adequate electronic contact between the current collector and the active mass.

2nd stage of evolution:

15 deep discharge cycles.
Capacity: 7 Sb: 2.150 Ah ; CaSn: 1.450 Ah;
CaSn/Sb = 0.67

The CaSn electrode has now entered into a phase of rapid irreversible capacity decay whereas the Sb electrode behaves normally.

Fig. 85 (a - b - c -d) again shows the interface grid-active mass at low and high magnification. With the CaSn electrodes, the delamination fractures are visible and, according to the observed decay of capacity, have probably increased in extension and severity. Fig. 86 (a - b - c - d) shows in greater detail the interface region with the good AM-CCL bond in the 7 Sb electrode and the ~6 µm gap and sulfated contact bridges in the CaSn electrode.

c and d represent the XRMPS of sulfur, again evidencing the sulfate formation in the interface CCL-AM of the CaSn electrode. The sulfur scan visible in d, Nr. 1, has been carried out in location Nr. 1 of b. This allows an integration of optical and chemical analysis and therefore a better description of interface structures.

These failing electrodes are now submitted to an acceleration of the disruptive process. In fact, the failing electrodes are treated, in terms of charge, to the same regime as the regular sister electrodes. This also represents conditions encountered in a battery when single elements or plates are failing in an accelerated way.

The amount of overcharge, initially ~15 - 20%, increased proportionally with the loss of discharge capacity and the electrode experiences high anodic potentials and gas evolution for a longer period as shown schematically in Fig. 87.

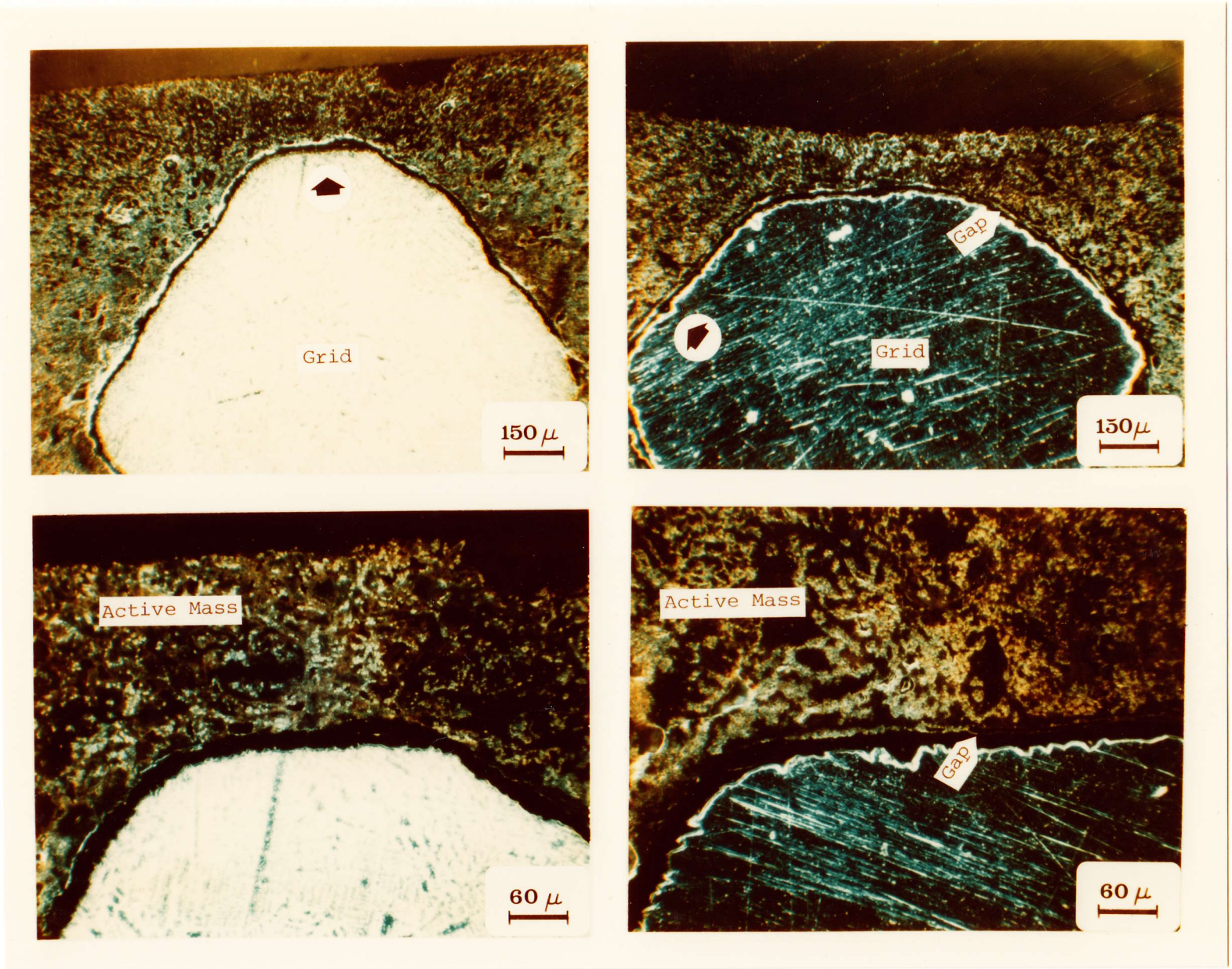

Fig. 85 | a | b | / | c | d | 2nd stage of evolution - 15 deep discharge cycles - fully discharged status.
a,c 7 Sb electrode - b,d CaSn electrode.

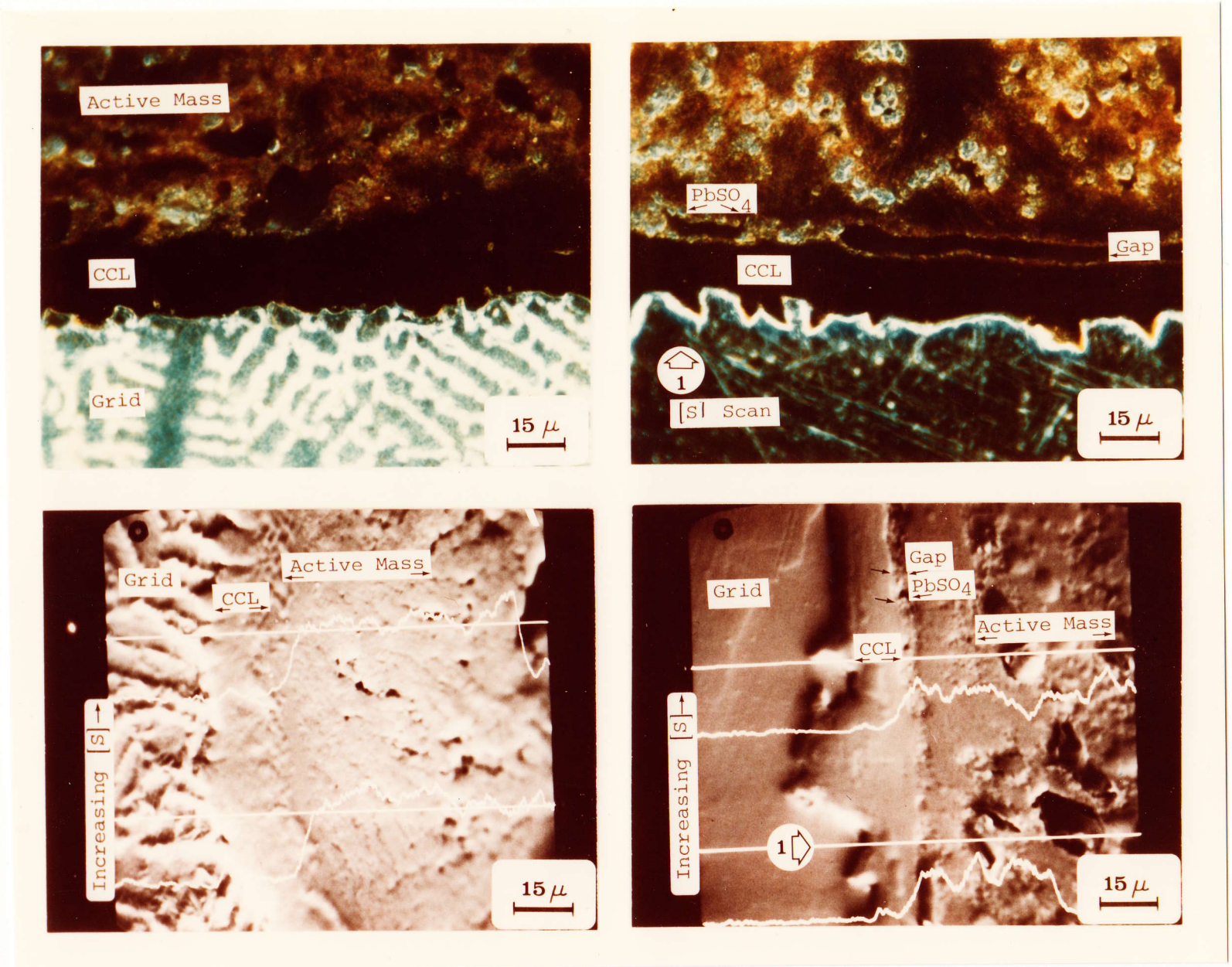

Fig. 86 | a | b | c | d |

2^{nd} stage of evolution - 15 deep discharge cycles - fully discharged status.

a,c 7 Sb electrode - b,d CaSn electrode.

72 c

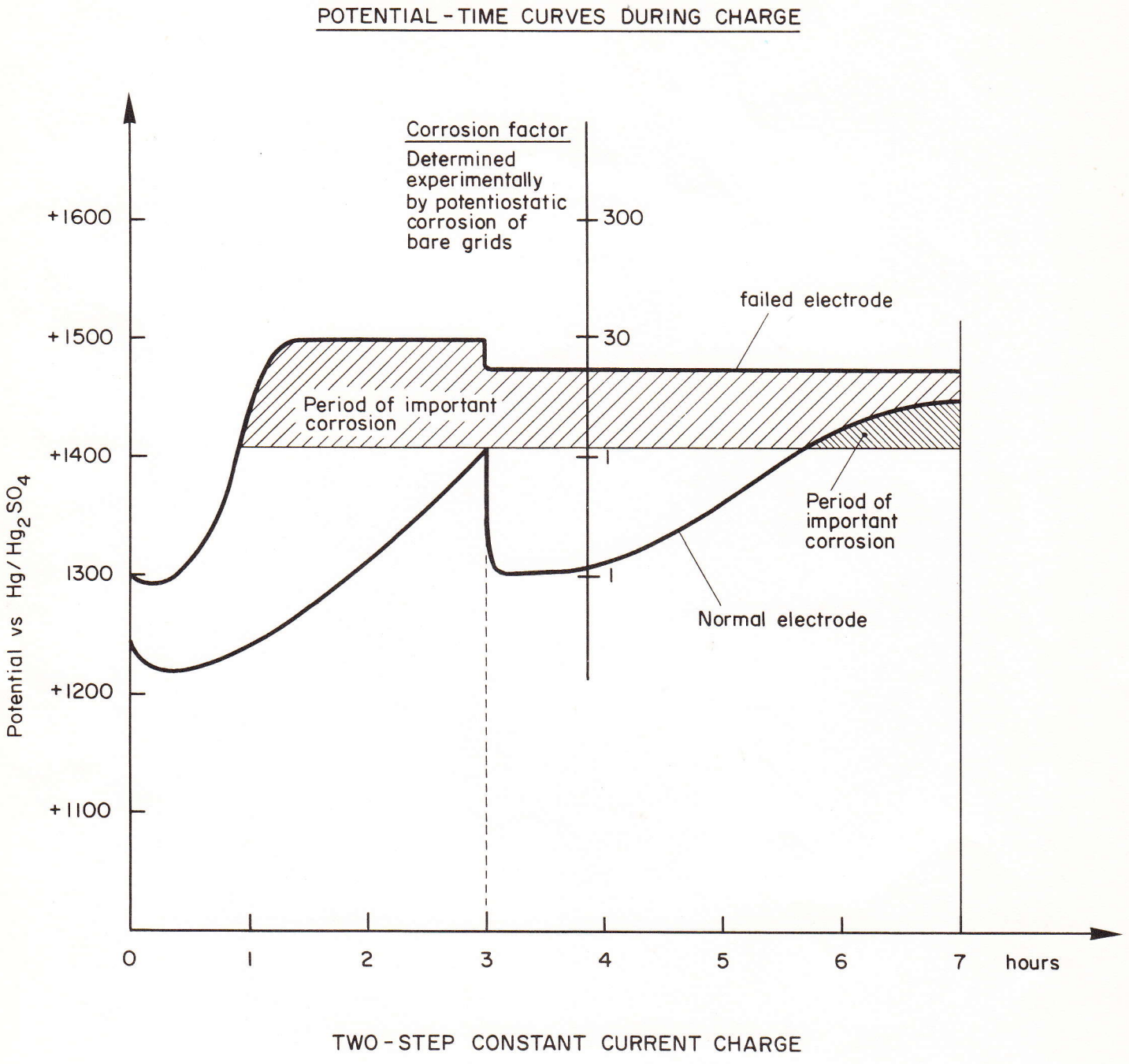

Fig. 87 Potential evolution of a failed electrode. Regions of increased corrosion.

The prolonged time at high anodic potentials increases the corrosion of the grid. As previous experience has shown, this corrosion product, growing at a high rate and in the absence of antimony, is of low cohesive strength and finely dispersed. This induces a two-fold damage in the interface. First of all, a PbO_2 of lower binding properties is produced as if it were grown in the presence of Sb and secondly,this fine PbO_2 is a choice site for the discharge reaction. The evolution of the interface of such samples will be shown in the next pages.

3rd stage of evolution:

40 deep discharge cylces.

Capacity: 7 Sb or CaSn (good): 2.000 Ah ;

CaSn (failed): 0.400 Ah ; CaSn/7 Sb = 0.2.

The CaSn electrode with the early failure-Sb^{II} effect now shows only a residual capacity of ~0.4 Ah, whereas electrodes with a Sb-grid alloy or a good CaSn electrode still yield ~5 x more capacity. The following figures will specify the relevant structure and $PbSO_4$ distribution in such electrodes.

Fig. 88 (a - b - c - d) shows the relative interfaces after 40 elapsed cycles of a "good" (a) and a "bad" (b) CaSn electrode. The failed CaSn electrodes, functioning in parallel with the good ones, were submitted to a heavy overcharge and related high anodic potentials as of the 20th cycle. Fig. c and d show the differences resulting from this treatment. The "failed" CaSn electrode shows a disintegrating corrosion layer, partially converted to $PbSO_4$ and evidence of large gaps between the CCL and the AM, whereas with the "good" CaSn electrode shown,no such features are visible. This is further shown in Fig. 89 a and b.

c and d show the sulfur XRMPS through these interfaces. The failed CaSn electrode shows an interface with a heavy $PbSO_4$ concentration in the CCL right down to the grid as evident by the $PbSO_4$ spikes visible in d.

This means that the bond active mass-grid, i.e. the CCL constitutes a site of discharge reactions which

(a) produce an isolating $PbSO_4$ film, and

(b) during charge, further disrupt the contact AM-grid with the formation of loose PbO_2 particles.

The status of the interface under fully charged and fully discharged conditions of a "good" and a failed CaSn electrode is shown in Fig. 90 a - b and c - d respectively.

Fig. d particularly reveals the transformation of the once compact CCL-PbO_2 into a $PbSO_4$ percolated structure. A major part of the electrode capacity now comes from this region, as the rest of the active mass has substantially lost all its electronic contact with the grid early during the discharge.

Fig. 91 reveals the uneven $PbSO_4$ distribution in failed CaSn electrodes.

a and b show the sulfur-XRMPS through sections of the electrode in the fully discharged status, i.e. the electrode reached +500 mV when a current of 600 mA/electrode was imposed.

In a, we notice from the two line scans that the sulfur, i.e. $PbSO_4$, is regularly distributed through the mass, a distribution which is confirmed by c, the sulfur-XRM-Area Scan of the same sample (rotated anticlockwise by 90°). This sulfur signal corresponds to

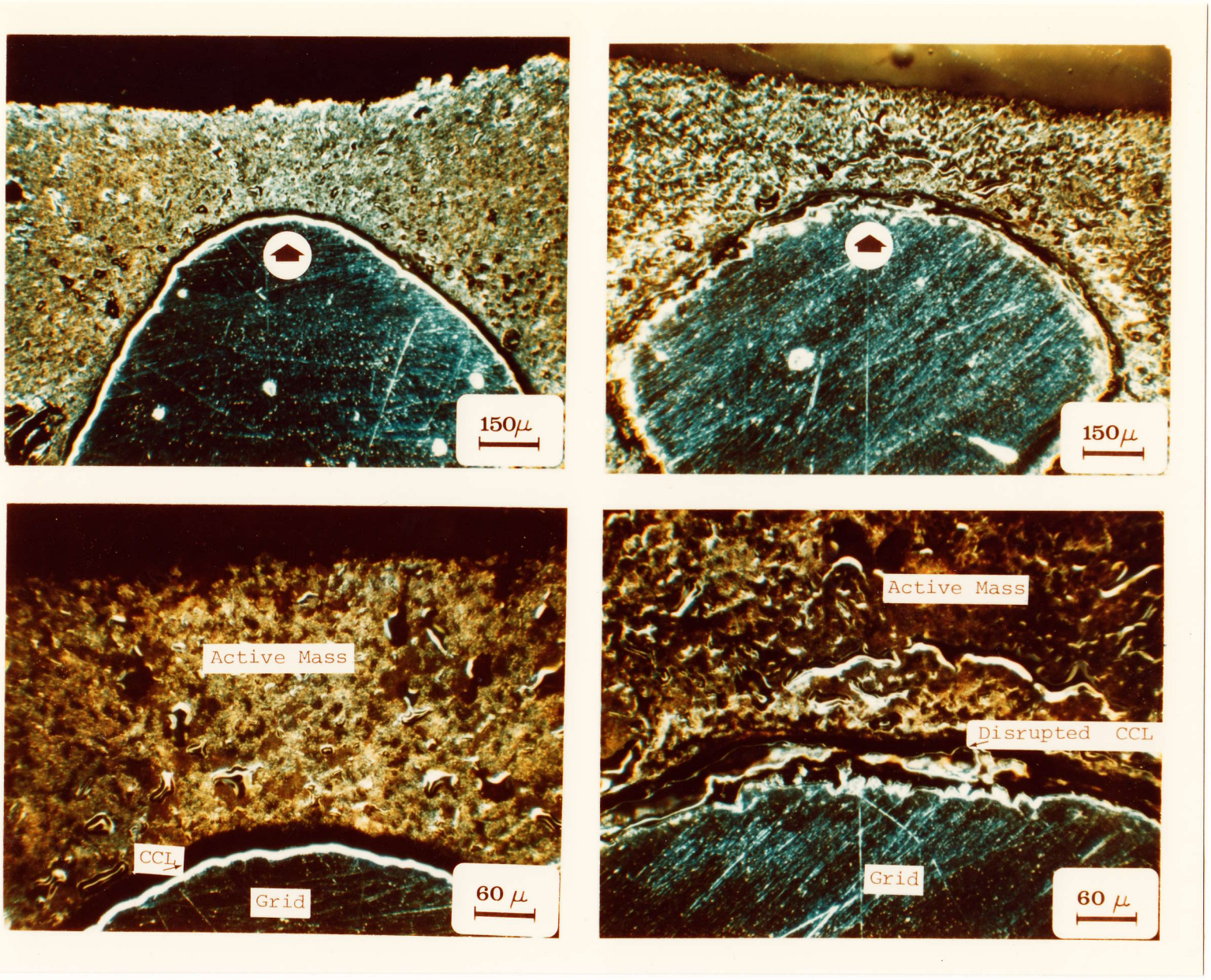

Fig. 88 | a | b | c | d |

3rd stage of evolution - 40 deep discharge cycles - fully discharged status.
a,c "good" CaSn electrode - b,d "failed" CaSn electrode.

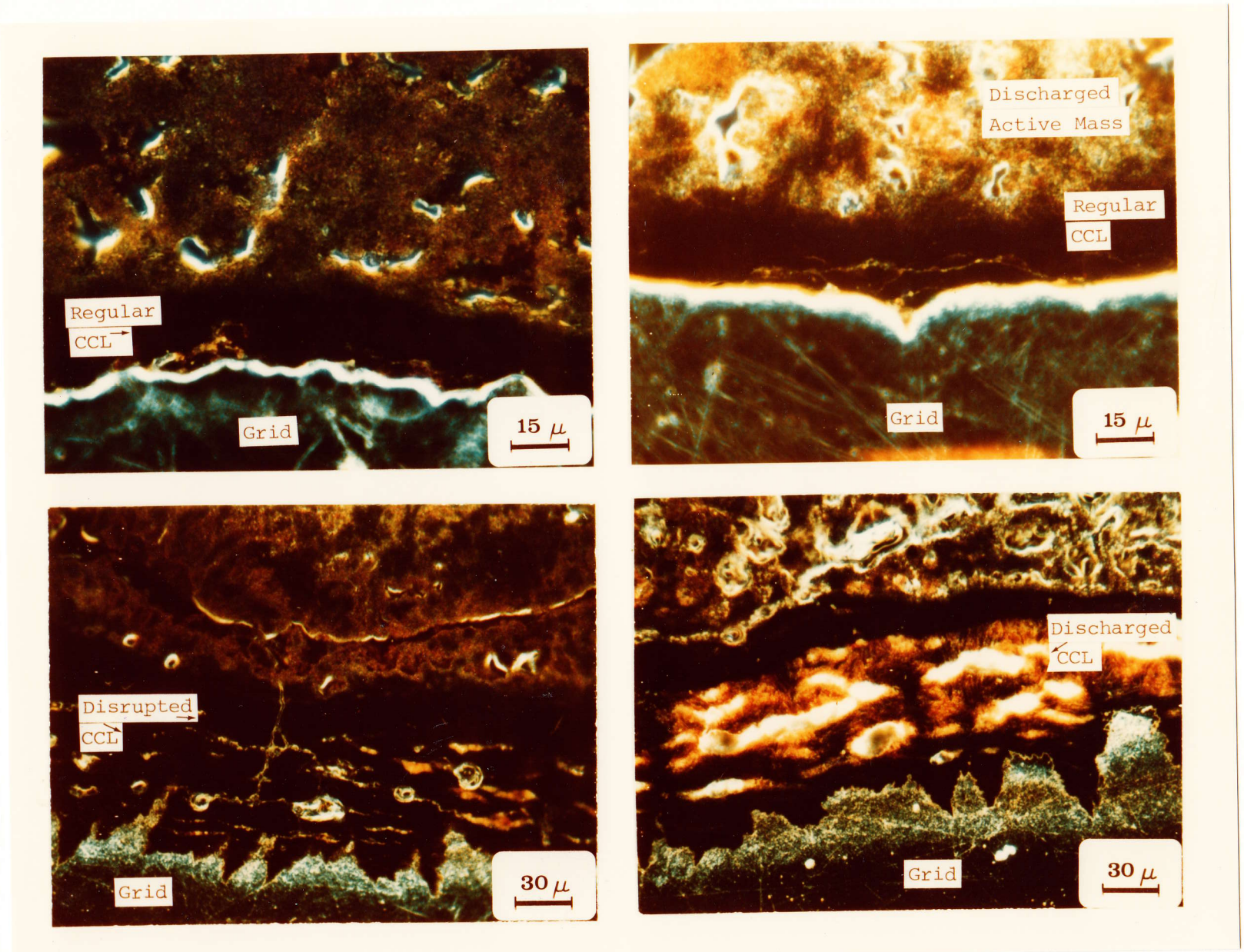

Fig. 90 | a | b | c | d |

Status of interface-CCL - fully charged and discharged status.
a,b "good" CaSn electrode - c,d "failed" CaSn electrode (40 cycles).

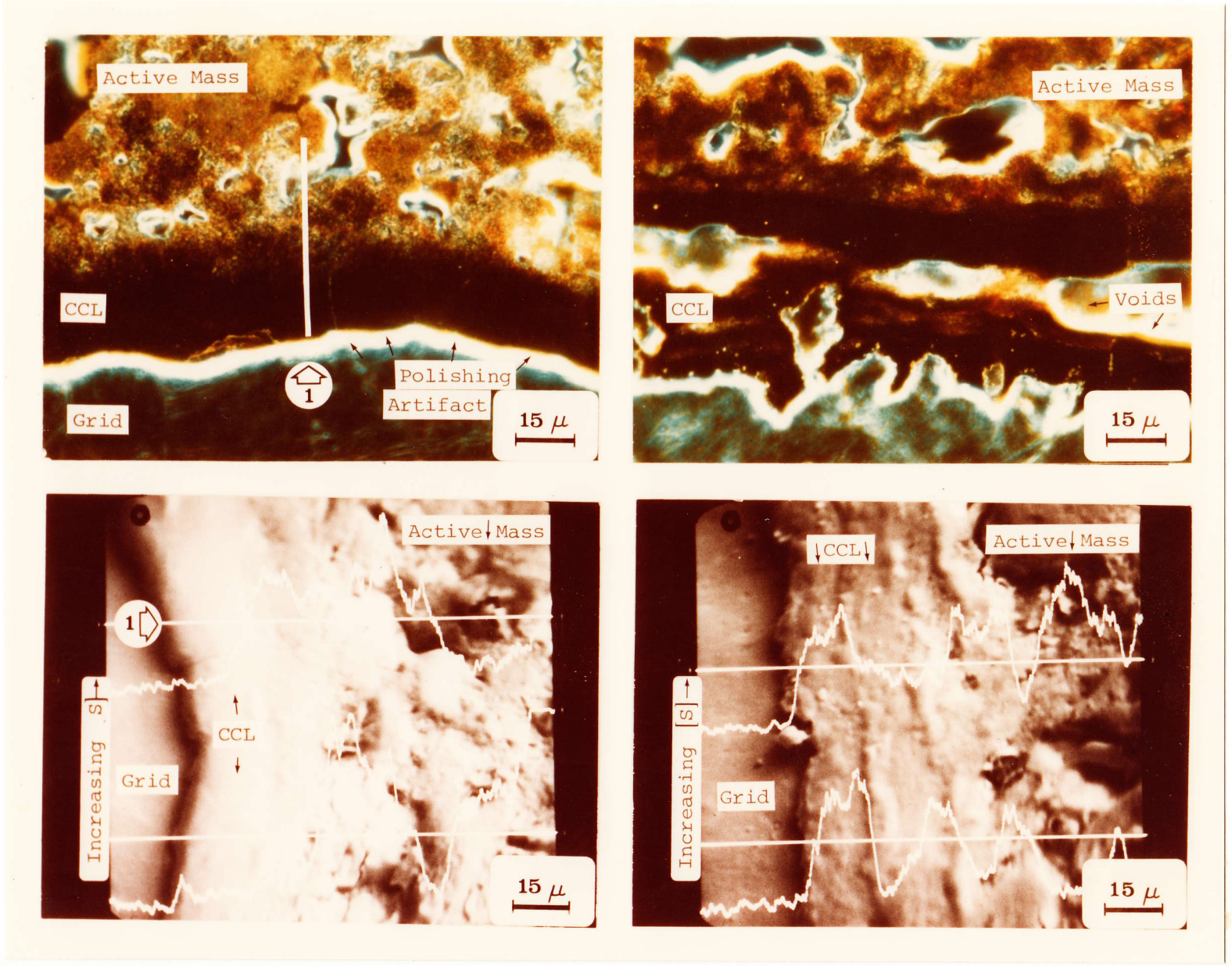

Fig 89 **a** **b** / **c** **d** 3rd stage of evolution - 40 deep discharge cycles - fully discharged status.
a,c "good" CaSn electrode - b,d "failed" CaSn electrode.

the extracted 2 Ah, i.e. the conversion of an equivalent quantity of PbO_2 into $PbSO_4$. The failed CaSn electrode, on the contrary, shows in b a heavy accumulation of sulfur, i.e. $PbSO_4$, in the vicinity of the grid and, more precisely, in the disrupted CCL. The XRMAS clearly indicates the $PbSO_4$ sulfate ring area which supplied part of the extracted 0.4 Ah. Some sulfate is also present in the active mass at the edge of the electrode toward the electrolyte. This indicates that the discharge simultaneously occurs in the exterior of the active mass (normal) and in the grid-AM interface (abnormal) with the latter discharge reaction apparently choking the electrode to death.

The ring of $PbSO_4$ as noticed in this particular case, i.e. early failure, is similar to the $PbSO_4$ rings reported by TUDOR et al. (J. Electrochemical Soc., 5, p. 21 (1967)) and REBER et al. (BOSCH Techn. Ber., 2, p. 159 (1968)). In view of the observed evolution of the interface, we consider this $PbSO_4$ ring to represent in the present case the final stage, i.e. EOL of the particular electrode, but not the intrinsic failure mechanism. This $PbSO_4$ is the result of a loss of contact with the active mass and related heavy overcharge which means that the Ah extracted now preferentially comes from the only PbO_2 body still sufficiently attached to the grid, the CCL. This produces a very localized $PbSO_4$ concentration profile as apparent in Fig. 91 b to d.

To recapitulate the know-how we have accumulated, we can now indicate that

(a) The seat of failure of certain CaSn electrodes (Sb^{II} effect) is concentrated in the interface grid-active mass.

(b) This failure is initiated by the formation of a low strength bond or gap between the corrosion layer-CCL and the active mass. This bond failure can be introduced during curing

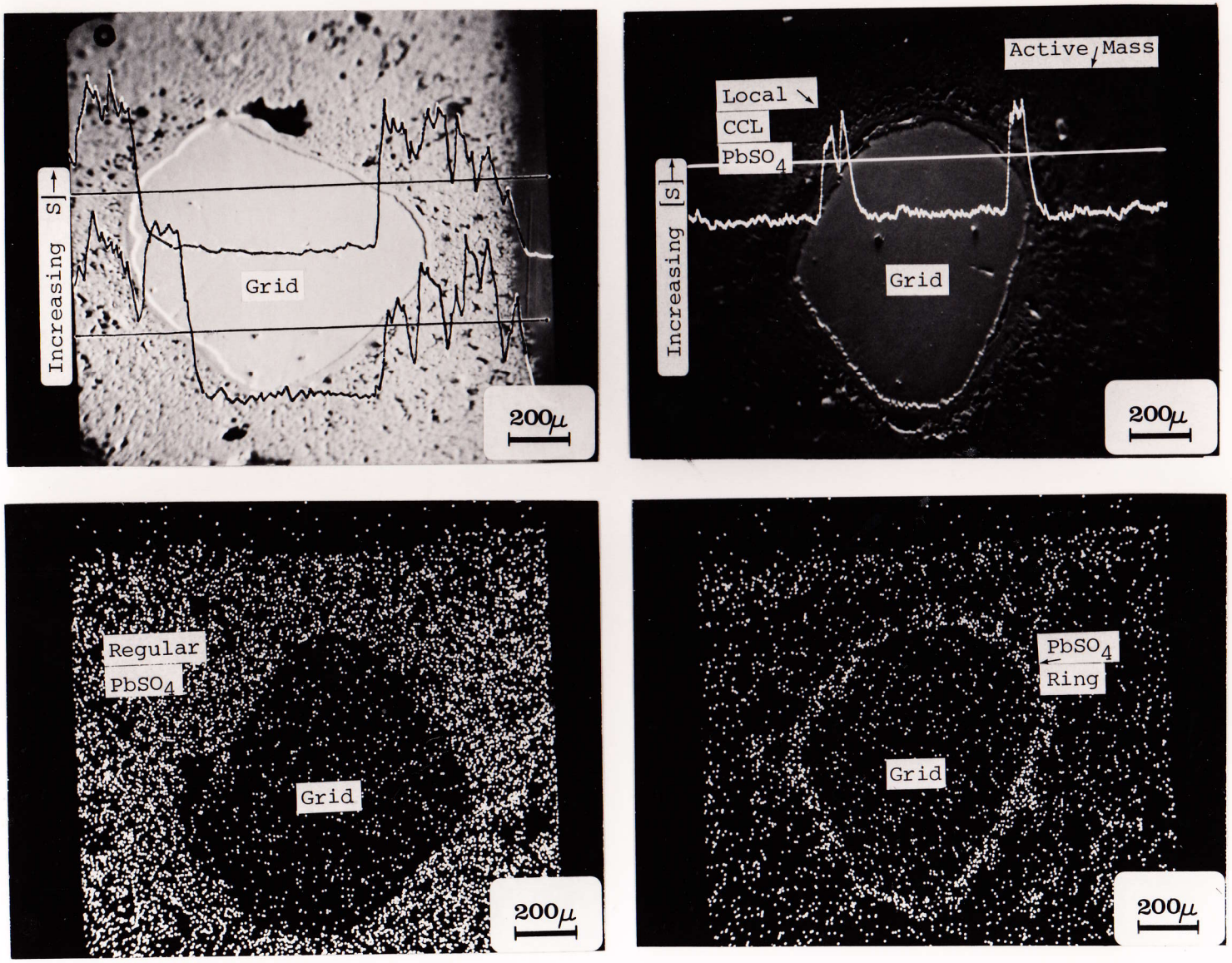

Fig. 91 | a | b | c | d |

Sulfate distribution - fully discharged status - XRMPS and XRMAS.
a,c "good" CaSn electrode - b,d "failed" CaSn electrode (40 cycles).

(shrinkage) and is accentuated by the fact that the PbO_2 which crystallizes during formation is finely dispersed and of low cohesive strength, i.e. exactly the opposite of what happens in the presence of Sb in adequate quantities.

(c) The capacity decay is accelerated by the continued destruction of points of sufficient electronic contact between the grid-CCL and the active mass.

(d) The resulting heavy overcharge and intensified discharge of the CCL results in a general disruption of the interface and the appearance of a $PbSO_4$ ring around the grid.

This $PbSO_4$ ring represents the nearly complete transformation of the once compact CCL-PbO_2 into an open active mass like PbO_2. Approximately 60% of the residual capacity of the electrode is now derived from the CCL-PbO_2, resulting in a typical ring profile of $PbSO_4$ around the grid.

This above experimental material gives a fair description of the phenomena which occur . We have completed these descriptions, as presented below, with experiments designed to selectively indicate the individual steps of such an early failure, especially with a view to further elucidating the role of Sb. Furthermore, we have looked for alternative scenarios, especially those which postulate the formation of an insulating film.

Alternative hypothesis for the Sb^{II} effect

The alternative hypothesis which could be made to explain the observed "early failure - Sb^{II} effect", is the formation of:

(a) an isolating film of $PbSO_4$ in the CCL-AM interface without any other collateral damage and as the sole and principal failure mode, and

(b) the formation of a film of PbO in the CCL-grid interface, due to the abnormal corrosion of the grid alloy in the absence of antimony.

The second hypothesis is particularly attractive as certain experimental data would allow an interpretation favourable to support such PbO film formation.

$PbSO_4$ in CCL-AM interface

This experimentally observed localized $PbSO_4$ accumulation also discussed in literature is *not the cause but the result* of other damages to the interface and instigates an early failure of the Sb-free electrode. $PbSO_4$ is indeed formed in the interface to a proportionally higher extent than in other active mass regions, but this is caused by the fact that these PbO_2 regions become less and less accessible for electrons,as in the interface highly resistive structures such as gaps and $PbSO_4$-PbO_2 masses are built up. Polarization measurements at the start of a new charge have revealed no abnormal polarization, such as for example:

7 Sb electrode - previous extracted capacity: 2.2 Ah
potential of the electrode
under 600 mA charging current: + 1296 - +1303 mV
(peaking after 30 s of charge)

CaSn electrode - previous extracted capacity: 0.97 Ah (failed)
potential of the electrode
under 600 mA charging current: +1298 - +1307 mV
(peaking after 30 s of charge)

As a microstructural investigation also confirmed, this interface $PbSO_4$ is completely and easily oxidized to PbO_2 without an additional or excessive polarization. We therefore exclude the formation of "hard" or irreversible $PbSO_4$ formation.

PbO in the CCL-grid interface

This hypothesis is based on the postulate that, under deep discharge conditions, the grid alloy without antimony produces PbO as a principal constituent of the corrosion product (see the theoretical basis for such PbO in the papers of RUETSCHI-PAVLOV-VALERIOTE). In order to confirm this thesis, it would be required that electrodes with Sb in the alloy never show an early failure, i.e. an Sb^{II} effect, as the critical interface in this hypothesis is the CCL-alloy interface. As a Sb-alloy contains antimony available in the grid-CCL interface independently of outside factors, such as coatings and fractures, the prevention of PbO formation or the "Sb doping" of PbO is always assured.

We have designed two reproducible experiments, 7Sb-Au coating and 5Sb-preanodized, where the early failures or the Sb^{II} effect are present, which therefore makes it unlikely that the above thesis applies in explaining the Sb^{II} effect - early failures (see data below).

Further investigations concerning the Sb^{II} effect

The precise localization of the Sb^{II} effect and the confirmation of its principal cause, i.e. contact loss between the grid-active mass, was further pursued with the following experimental sets:

(a) deliberate introduction of fractures in the interface active mass-grid in combination with other damaging factors such as inert (gold) or rapidly dissolving (cadmium) coatings;

(b) the surface Sb depletion of Sb alloy grids to eliminate the Sb fraction active during curing and formation;

(c) artificial Sb introduction in the positive electrode;

(d) the evaluation of a perfected curing technique, such as the DELCO-GM process, to improve active mass adhesion;

(e) the evaluation of an appropriate charging technique, such as current limited constant voltage charging.

These experiments will be presented below:

(a) Deliberate introduction of fractures

Inert or dissolving coatings on the grid.

Selected grids were gold (4 or 40 µm Au) or cadmium (15 µm Cd) plated. These electrodes were all pasted with the same batch of paste.

In order to accentuate fractures, replicate electrodes were held for 5 minutes at 60°C in dry air. This introduced numerous shrinkage fractures in the mass pellet. These fractures were visible practically in every mass pellet and substantially extended through the entire circumference of the pellet, i.e. the interface active mass-grid. The artificially introduced shrinkage fractures were much the same as those commonly observed on industrially prepared positive electrodes (particularly thin and SLI plates). After this treatment, the samples were cured as usual.

After formation, where no difference in behaviour was observable in terms of incomplete conversion into PbO_2, the electrodes were cycled to +500 mV discharge potential and ~20% overcharge. The monitoring of the capacity first gave the confirmation of the Sb^I effect (see previous chapter) and then showed the different behaviours of the specific electrodes. In Fig. 92 the presented capacity decays are typical and represent the mean behaviour of 6 replicate electrodes.

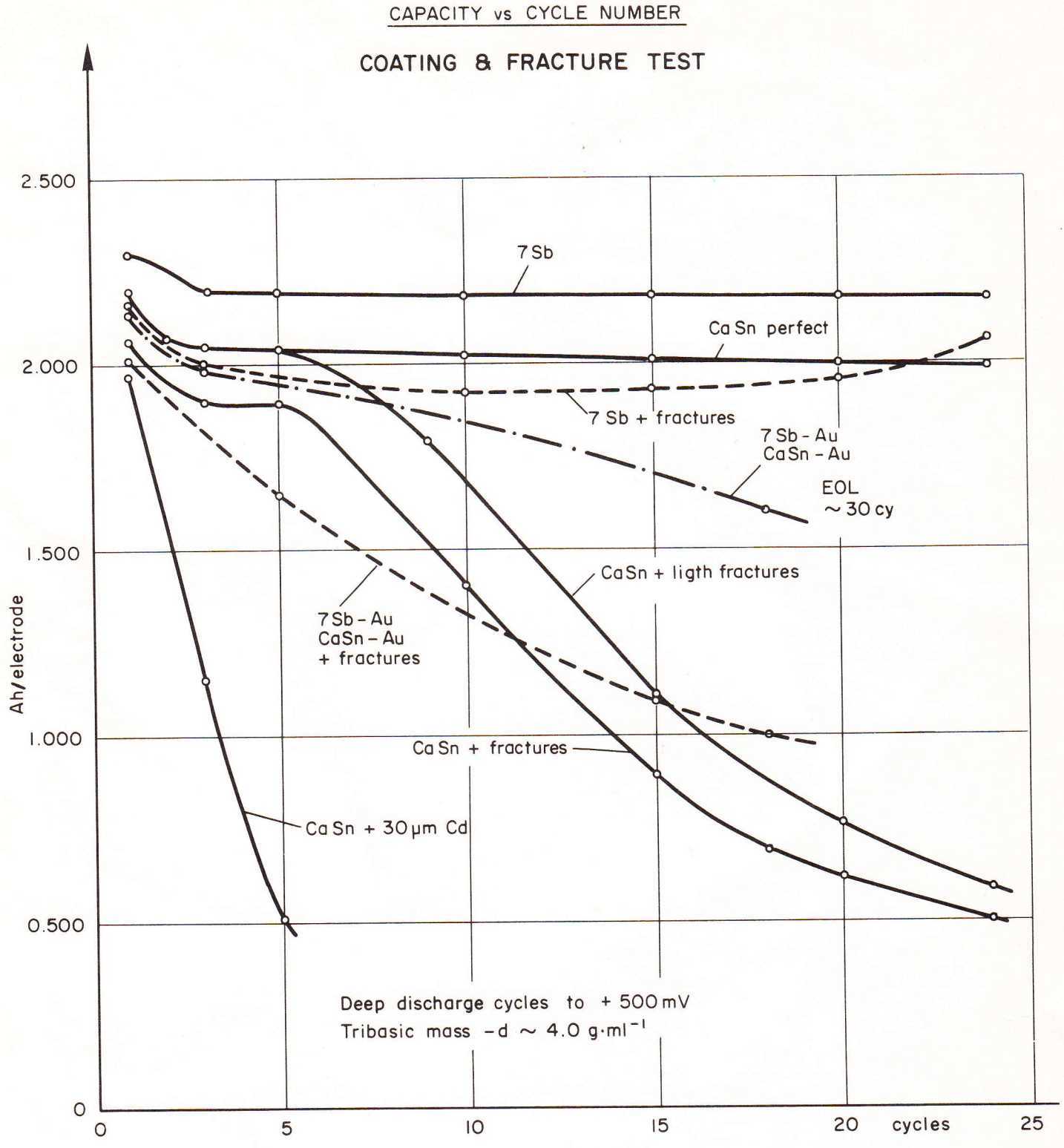

Fig. 92 Evolution of capacity in function of interface status modifications introduced to induce the Sb^{II} - early failure effect.

7 Sb electrodes (7 Sb)

The antimony containing grid electrode shows a substantially flat capacity vs cycle behaviour although slight fractures were present in the electrodes.

7 Sb + fractures

The only consequence of the severe shrinkage fractures introduced by the drying was a depression of the capacity without introduction of any early failure. Also noticeable was a capacity recovery to nearly normal, i.e., the "healing" observable during the later stages of cycle life.

CaSn perfect - CaSn light fracture - CaSn + fractures

CaSn perfect represents the behaviour of successfully cycled CaSn electrodes without any relatable gross shrinkage damage.

The CaSn electrodes with *light fractures* and *fractures* originating from the additional "hard" drying, both show a 100% failure rate, i.e. 6 out of 6 show the Sb^{II} early failure effect. We observe that the additional cracking introduced depresses the capacity further but that the onset of the rapid capacity decay is very similar.

Samples with Au coating

In order to weigh the relative importance of the grid-CCL-active mass interaction as a function of the availability of antimony in the interface, samples with Au coating were cycled simultaneously with the above sets.

The result was that samples with a 4 µm Au coating without additional cracking failed in approximately 30 cycles (EOL 50% capacity loss) without any distinction between a 7 Sb and CaSn grid

base. This is particularly interesting as the 4 µm Au coating was perforated (i.e. pinholes present) and the grid alloy was corroded underneath. The possible Sb release from the 7 Sb grid into the disintegrating interface active mass-grid and into the active mass itself, was not sufficient to counterbalance the capacity decay. Samples with a 40 µm Au coating without additional cracking failed in approximately 30 cycles without any distinction between the 7 Sb and CaSn grid base. In this case, the thick gold coating was impervious and no corrosion of the base lead alloy occurred.

The surprising observation was that the capacity decay (see Fig. 92) was much more gradual than those observed with bare fractured CaSn grids, i.e. ~0.05 $Ah \cdot cycle^{-1}$ with Au coatings vs ~0.12 $Ah \cdot cycle^{-1}$ with bare CaSn grids.

This would confirm that the adhesion and/or bond formation (Sb^{II} effect) is influenced in CaSn electrodes by the "reactivity" of the CaSn alloy surface. In fact, the Au coating does prevent any oxidation of the grid during curing and formation, but not during cycling, as in the case with the 4 µm Au coating. It seems that the interface status, which is responsible for the non-occurrence of the Sb^{II} effect, is prevented by the presence of gold, under mild fracture conditions.

When additional fracturing is introduced, 7 Sb-Au + CaSn-Au (fractures) (see Fig. 92), then the previously surviving bond or interface status is destroyed and the gold coated electrodes show an immediate and rapid capacity decay.

The failure of the Au coating electrodes confirms that a delicate balance of the interface conditions must be maintained if Sb is not available in adequate quantities at the right moment (formation) to counteract the specific failure mode.

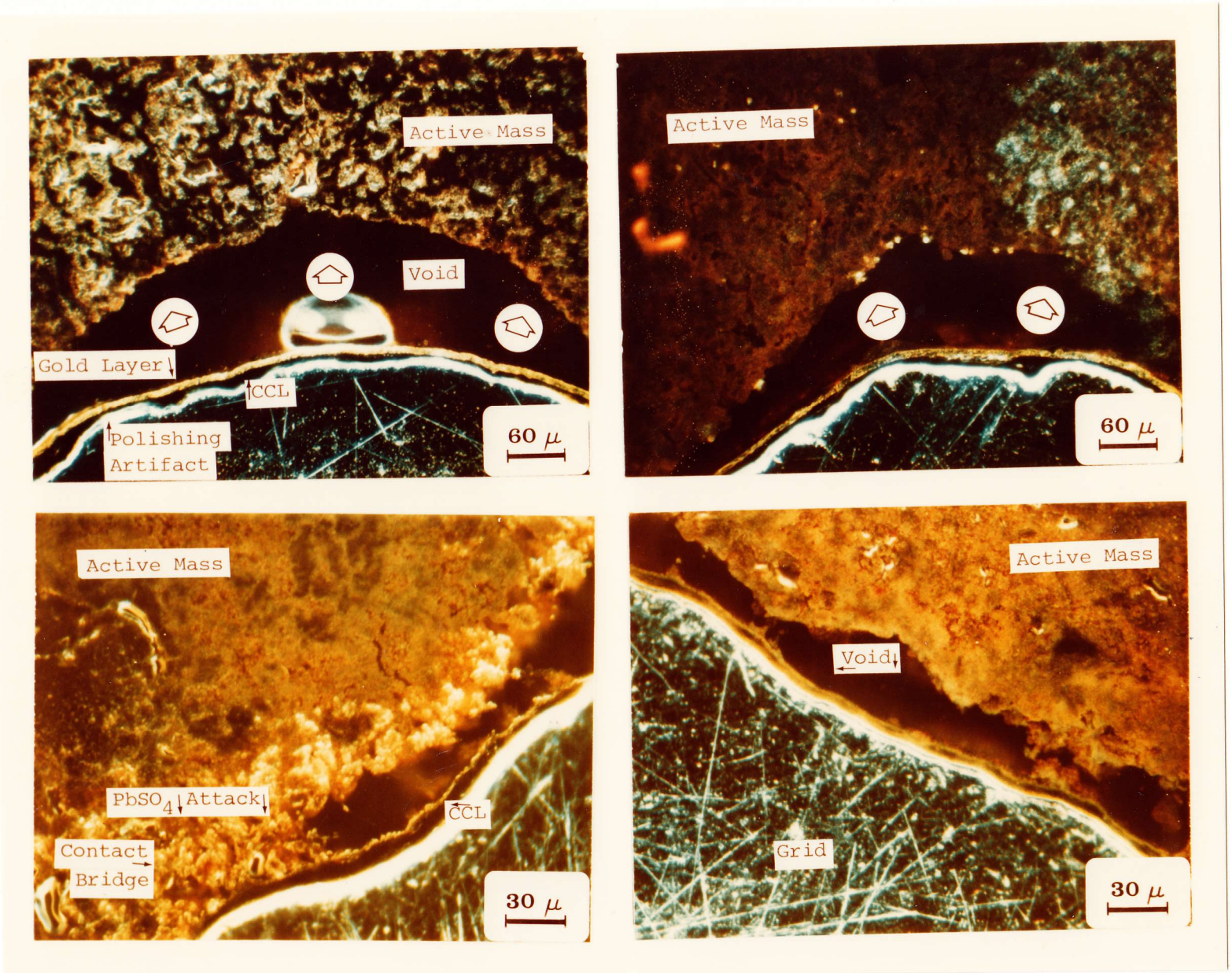

Fig. 93 **a** **b** / **c** **d** Sb^{II} specific experiments - gold and cadmium coatings.
a,b gold coating - c,d cadmium coating.

Along with the cost of gold, the failure of these 40 µm gold electrodes within 30 cycles also precludes the use of such non-corroding grids under deep cycling applications. The failure mode of such electrodes can again be attributed to an interface phenomenon and characterized by the gradual "moving away" of the active mass from the grid. Typical interfaces of such samples are shown in Fig. 93 a - b, a the fully discharged and b the fully charged status. The typical large void formation in the interface is noticeable in both pictures.

Samples with Cd coating

A set of samples was also coated with 15 µm Cd in order to introduce a definite void volume into the interface by means of dissolving the Cd layer during formation and cycling. A very rapid capacity loss of ~0.35 Ah·cycle was recorded.

This loss of active mass to grid contact through void formation very much parallels the observed Sb^{II} effect phenomena.

Details of such interfaces are shown in Fig. 93 c - d, c in the fully discharged and d in the fully charged status, with 0.3 Ah per electrode of residual capacity. In both cases, only limited contact points between the active mass and the grid are observed.

(b) Surface antimony depleted 5 Sb grids

The release of oxidized antimony species into the interface grid-active mass occurs in three distinct periods, each period characterized by distinct Sb flow rates.

The first release occurs during curing through the very slight oxidation of the α-phase and the exposed β-phase. The Sb content in the α-phase is very low (Sb < 0.3% w/w), whereas the β-phase and

segregated excess Sb yield the principal flow through oxidation. The mobility of Sb_{ox} in the curing environment is rather low, but positive effects, duplicable with Sb_2O_3 additions, are seen in the improved adhesion.

The second Sb release occurs during the formation step and the connected grid corrosion. In a relatively short period, a concentrated Sb release is experienced, which coincides with the oxidation of a small interface volume from a $3PbO \cdot PbSO_4$ + PbO mixture into PbO_2. The PbO_2 structure grows in such a manner as to produce compact and well connected PbO_2 crystal colonies. The third Sb release slowly occurs during the cycling corrosion process and permeates the entire active mass during the periodic charge and discharge of the PbO_2-$PbSO_4$.

It was thus interesting to investigate which flows are the most critical for preventing early failures, i.e. the Sb^{II} effect.

We therefore preanodized clean 5 Sb and CaSn grid electrodes in 1.06 sp.gr. H_2SO_4 (pure or saturated in Sb_2O_3) for 20 h at 40°C and with 417 mA·electrode, thereby replicating similar current density and temperature conditions as observed during formation.

In the case of 5 Sb grids, the resulting PbO_2 layer was with or without Sb present in H_2SO_4, well adherent and of metallic luster. This metallic luster was given by the particular growth structure of PbO_2 detailed in the previous chapter. When prepared in the presence of Sb ions, the PbO_2 layer on CaSn electrodes was either similar to that observed with the 5 Sb grids or, in the absence of Sb, powdery brown without adherence.

The 6 replicate grids treated in this way were then pasted, cured and formed together with untreated 5 Sb electrodes. In addition to an Sb^{I} effect with the preanodized Sb grids, the Sb^{II} effect was also noted. The preanodized 5 Sb grids were prepared in two sets with a variable degree of shrinkage fractures. Fig. 94 specifies the relative capacity curves.

We observed that CaSn and the preanodized 5 Sb grids, independent of Sb in the preanodization acid,but with shrinkage fractures, rapidly failed showing the typical Sb^{II} effect phenomenon.

5 Sb preanodized grids, but with no shrinkage fractures, initially also showed a rapid capacity loss which gradually came to a halt and then reversed until the original capacity was restored.

We can infer the following from this experiment.

At the moment, we are not able to discern precisely if the existence of the preanodized PbO_2 layer or the absence of antimony during curing and formation contributed to initiating the observed failure. We note that the absence of formation antimony did not allow the damage introduced by the shrinkage fractures and the related change of the interface status,to be overcome. When this formation antimony was freely available as in test "7 Sb + fractures" (Fig. 92), no Sb^{II} effect was detectable.

In the experiment where these fractures were minimized, one still observes an initially rapid capacity decay of the electrode due to the extraneous interface PbO_2 (from preanodization) or due to the absence of formation-Sb. The subsequent heavy overcharge strongly increased the flow of the 3rd Sb type (from the cycling corrosion phenomena). This antimony flow appears to have "healed" the damage caused by the preanodization and Sb-leach, as a gradual restoration of the capacity was noted.

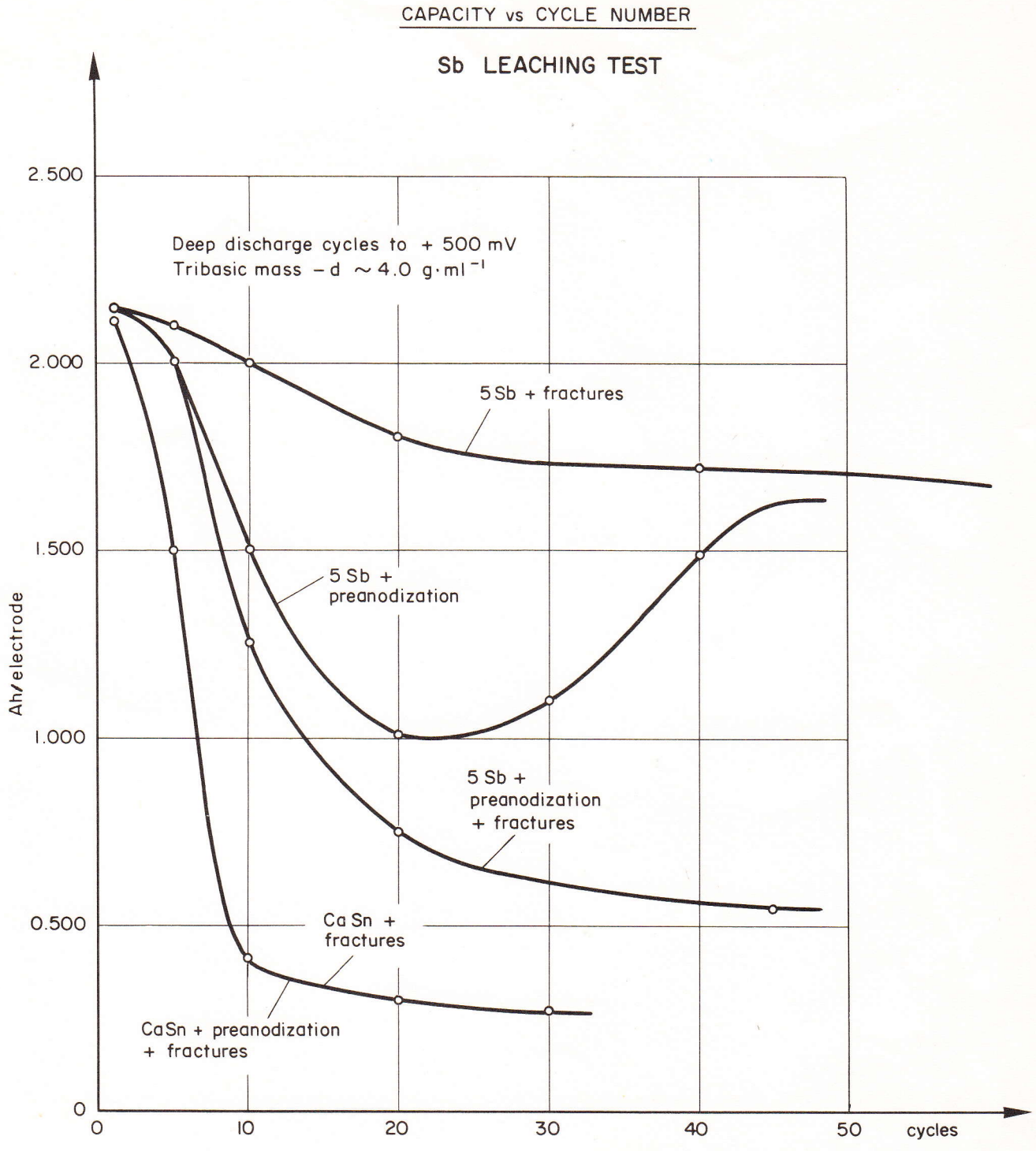

Fig. 94 Evolution of capacity in function of antimony release factors.

A precise description of this effect is still lacking but we presume that in the case of the presence of Sb ions, two separated PbO_2 surfaces might intergrow and allow a satisfactory electrical contact to be re-established between grid CCL and active mass. Crudely expressed, the presence of Sb ions in solution, absorbed or built into the PbO_2, would allow an improved "wetting" and intergrowth of two contiguous PbO_2 crystallites (lowering of the PbO_2-PbO_2 interface energy) as demonstrated also in Chapter 3.4.4.

Again, such an effect could also be active in the long term stabilization of the PbO_2, i.e. on the Sb^{III} effect.

The structures in the interfaces of such electrodes are shown in Fig. 95 a - b - c - d, Fig. 96 and Fig. 97 a - b - c - d.

Fig. 95 a - c shows the interfaces in the fully discharged conditions for the failed 5 Sb (preanodized) electrodes compared to a failed CaSn (normal) electrode in b - d after 19 cycles. Both interfaces are similar. One observes the presence of a ~60 µm large region around the grid permeated with $PbSO_4$, and fractures in the CCL and beyond the $PbSO_4$ ring. The active mass itself shows areas which participated in the discharge. This discharge is located in the exterior of the plate up to a depth of ~40 - 60 µm. We presume that contacts between the outer region of the mass exist at the beginning of the discharge, but as they are few and exposed to the discharge process, due to fractures and the absence of adequate Sb concentration, they transform prematurely or abnormally into insulating $PbSO_4$. This does not happen when an adequate Sb supply is available in this region or when the electrode manufacture did not induce drying fractures. Such a typical $PbSO_4$ distribution as noticed at EOL of an early failure CaSn electrode is shown in Fig. 96.

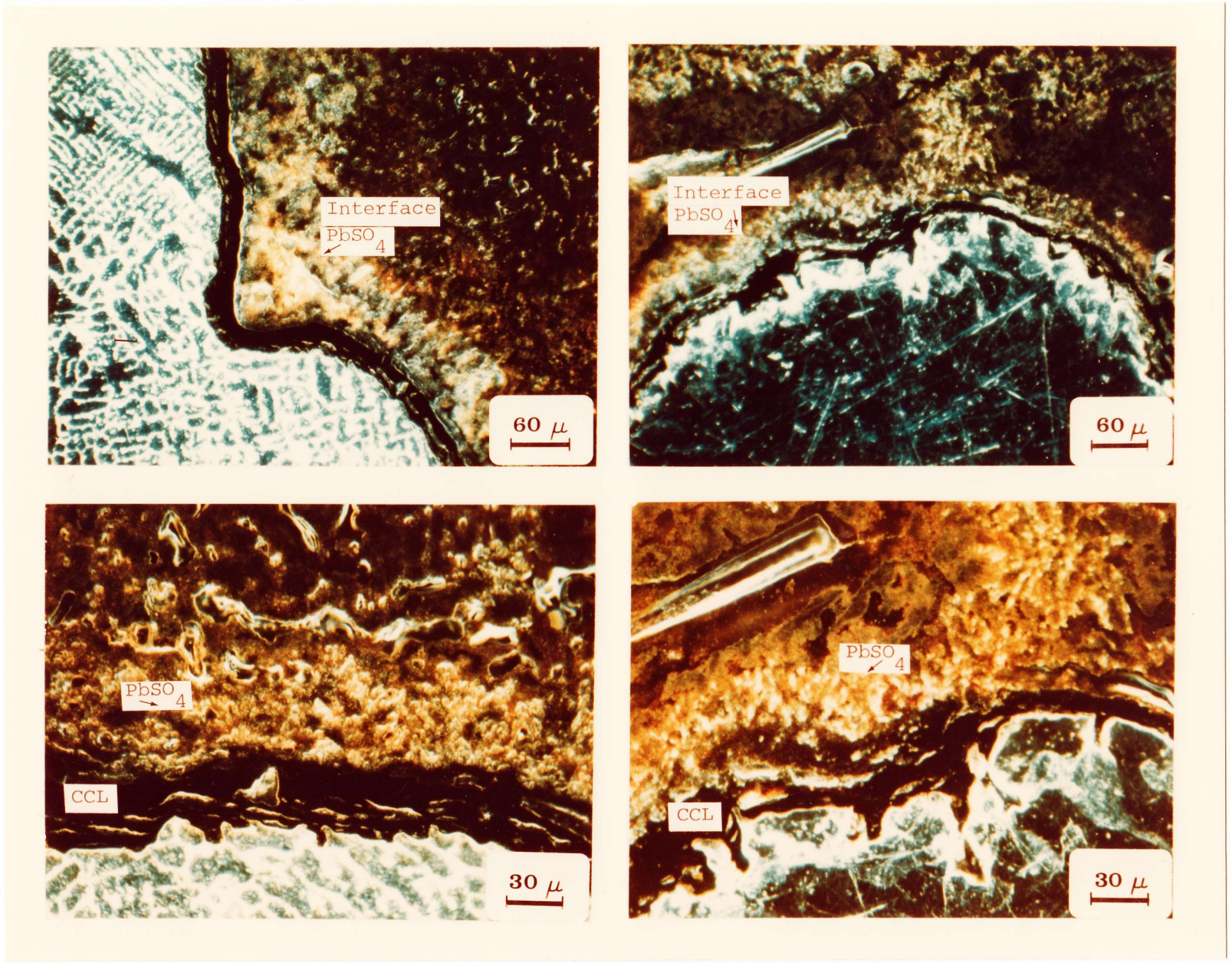

Fig. 95 **a** **b** / **c** **d** Preanodized grid electrodes - fully discharged status - 19 cycles.
a,c 5 Sb electrode - b,d CaSn electrode - both failed.

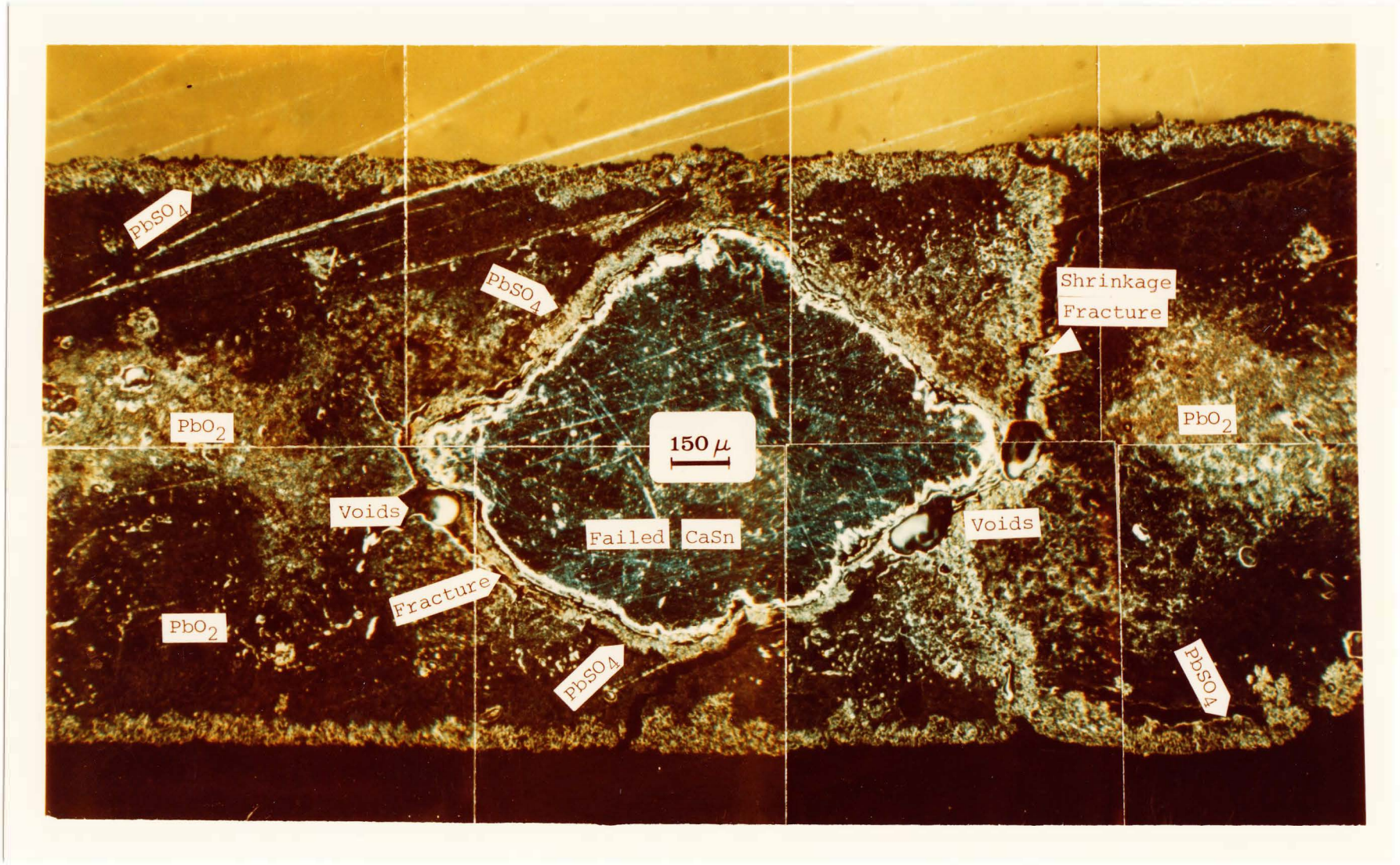

Fig. 96 Typical cross-section of a Sb^{II} effect failed CaSn electrode after 19 cycles. Note the $PbSO_4$ present in

a) the outer edges of the active mass,
b) along shrinkage fractures, and
c) around the grid member.

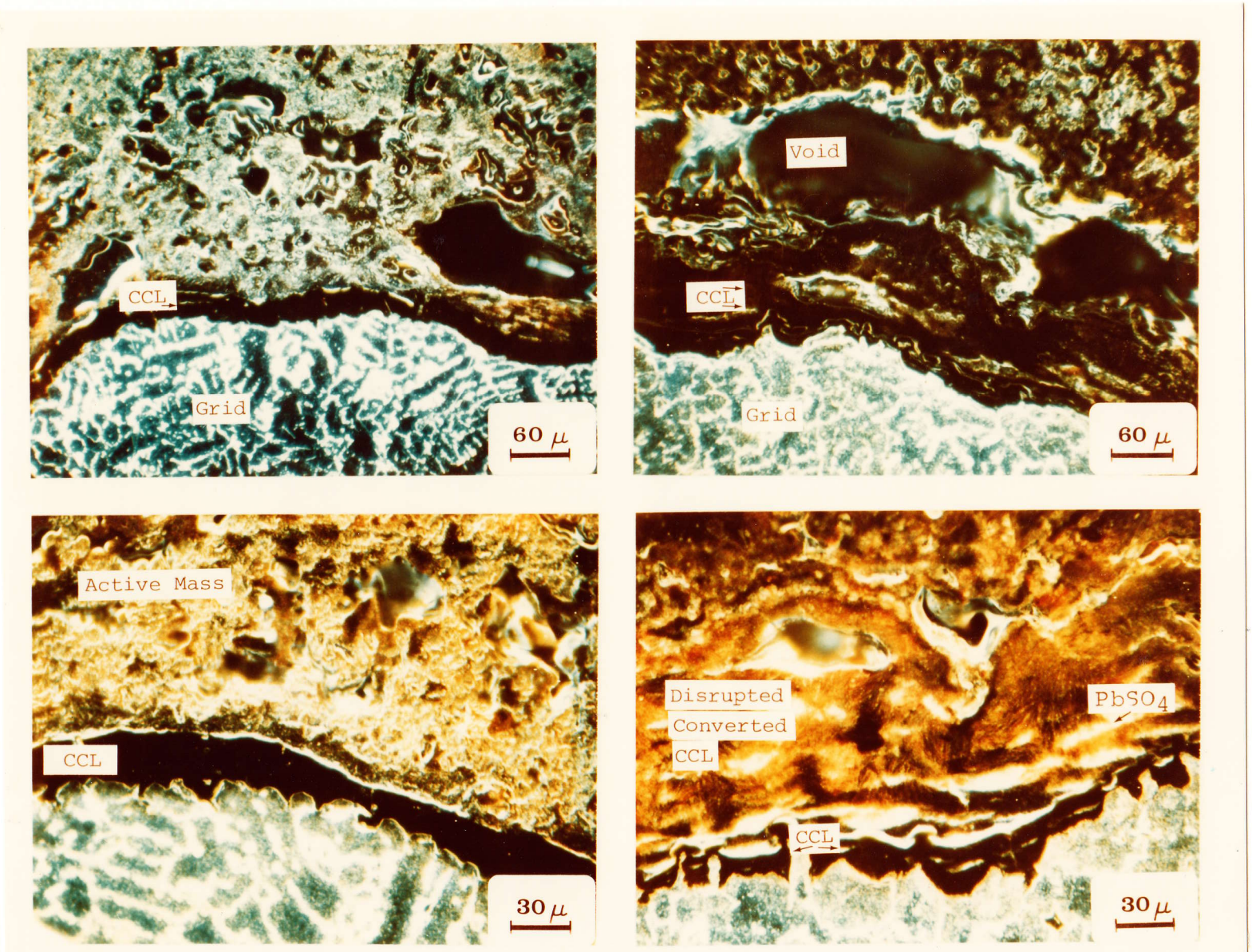

Fig. 97 | a | b | c | d | Comparative structures of 5 Sb electrodes - fully discharged status - 46 cycles.
a,c 5 Sb - normal structure, b,d 5 Sb-preanodized and failed electrode structure.

Fig. 97 a - b - c - d shows the further evolution of such interfaces now compared to an equivalent 5 Sb electrode after 46 deep discharge cycles. The preanodized and failed 5 Sb electrode shows a very disrupted interface with large voids and with the dislocated CCL transformed into $PbSO_4$ (Fig. b). The residual capacities at this stage are 1.8 Ah for a normal 5 Sb electrode and 0.6 Ah for a preanodized 5 Sb electrode.

(c) Artificial introduction of antimony into the positive electrode to prevent the Sb^{II} effect

Several attempts were made to artificially introduce Sb, with its beneficial effect, into the positive electrode. The intention was to bring a minimum of Sb into the selected regions, active mass or interface or both, as antimony metal, in order not to predetermine the valency of the resulting Sb ions, i.e. Sb^{III} or Sb^{IV} nor their relative proportion. In general, the results reflected a tendency to eliminate or delay the Sb^{II} effect, but the results obtained did not allow such a method to be recommended as an adequate way to avoid early failures.

Before discussing these tests, we would like to recall that any artificial Sb addition must maintain the integrity of the interface without introducing additional structure discontinuities therein. In fact, the dendritic nature of the solidification of the PbSb alloys is a very good compromise between areas with high Sb release and areas of contact. See also Fig. 98. The introduction of a Sb source, forcibly soluble to be effective, will weaken this critical region to the extent where antimony's positive effect is counterbalanced by the creation of an abnormal interface status. This was indeed the case with several experiments.

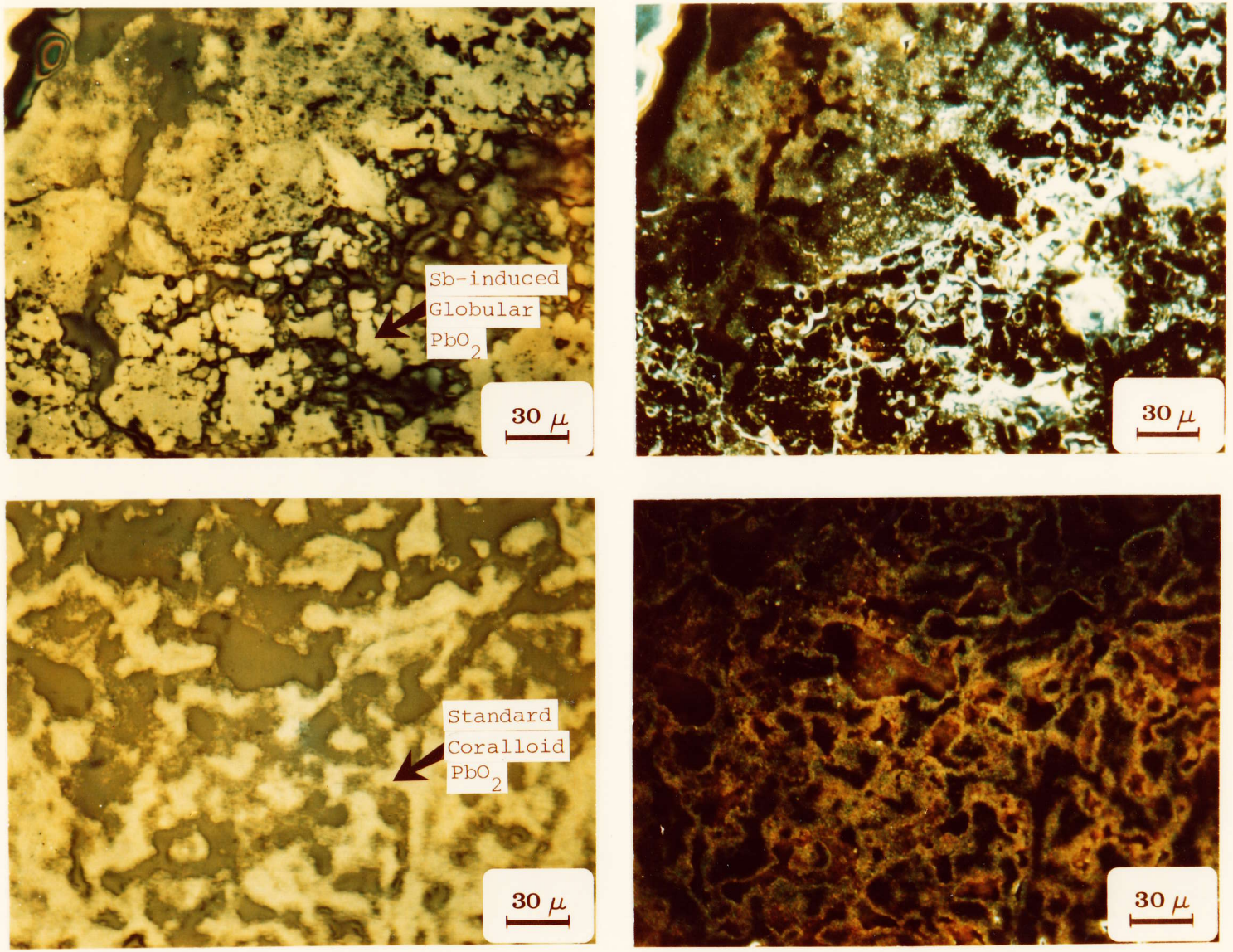

Fig 99 | a | b | c | d |

Artificial Sb introduction to prevent the Sb^{II} - early failure effect.
a,b globular Sb_2O_3-induced PbO_2, c,d coralloid PbO_2
(clearfield-darkfield illumination).

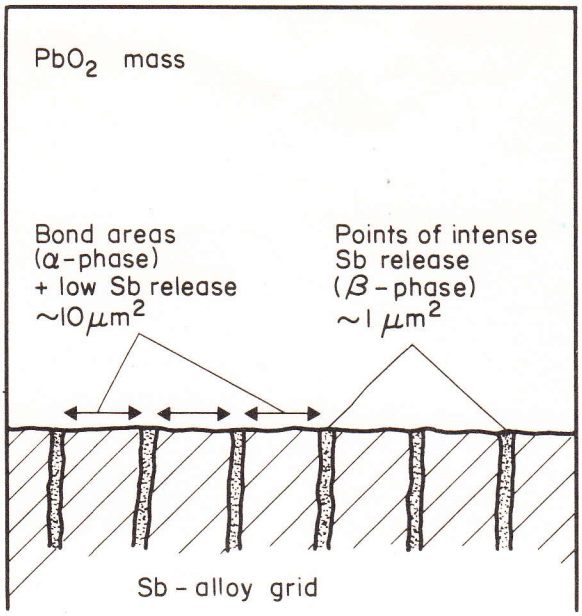

OPTIMAL BOND FORMATION
EFFECTIVE UNDER ALL CONDITIONS

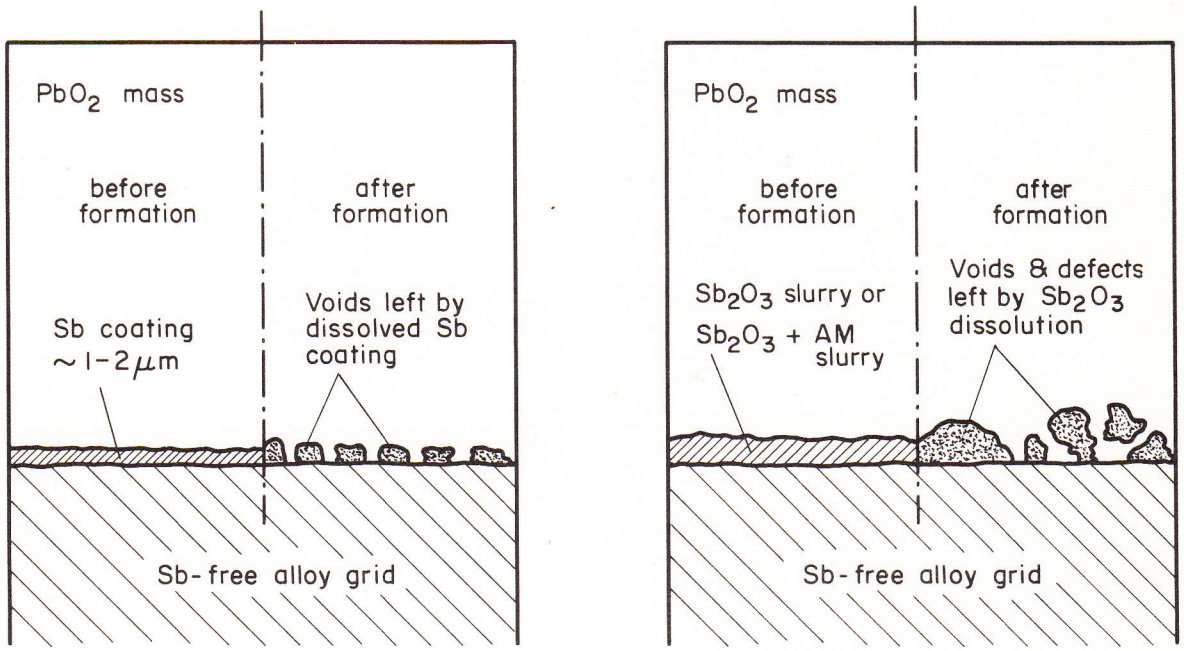

IMPROVED BOND FORMATION EFFECTIVE
ONLY IN NOT TO SEVERE CONDITIONS

Fig. 98 Antimony sources and related bond formation during curing and formation.

The following tests were carried out:

- 1.5 µm displacement coating on CaSn grids according to US Patent 3.933.524 (1976).

  Result: effective only when the type of electrode preparation itself already gives a low Sb^{II} effect related failure rate. Not effective with major shrinkage fracture damage.

- 0.2% w/w Sb metallic powder (30 µm grain size) mixed into the reacted paste.

  Result: most effective treatment of all tested combinations. Also prevents the Sb^{II} effect with CaSn electrodes where the untreated replicate batch showed a 100% failure rate.

- 0.2% w/w Sb as metallic Pb2%Sb powder (30 µm grain size) mixed into the reacted paste.

  Result: only one experiment was performed. No failure - Sb^{II} effect - encountered,but the sister batch also showed only minimal failures.

- CaSn grid preanodized in 1.06 sp.gr. H_2SO_4 (saturated in Sb_2O_3) for 20 h - 40°C and 417 mA·electrode.

  Result: negative result - all failed.

- Formation for 3 h in 1.06 sp.gr. H_2SO_4 saturated in Sb_2O_3 at 40°C and 187 mA·electrode, then change to pure 1.06 sp.gr. H_2SO_4 formation.

  Result: negative result - all failed.

- CaSn grid coated with a paste - Sb_2O_3 mixture before final pasting. Sb quantity introduced into the interface active mass-grid was ~0.03 - 0.04 g Sb·electrode.

  Result: improved specific capacity (Sb^{I} effect) but no prevention of the Sb^{II} effect.

- CaSn grid coated with a Sb_2O_3-water slurry before pasting. Sb quantity introduced into the interface active mass-grid: 0.21 to 0.26 g Sb·electrode.

  Result: delayed Sb^{II} effect, i.e. partially effective. But the presence of Sb_2O_3, carried by the free water of the paste into the interior of the pellet, prevented complete curing and formation and caused massive active mass disintegration. The positive effect was counterbalanced by the above side effects. The active mass in the electrode showed large colonies of very compact and globular PbO_2 of the same nature as the PbO_2 of the interface observed with Sb containing grids or PbO_2 crystallizing in the presence of Sb ions. These massive globular PbO_2 colonies were still recognizable after 32 discharge cycles which testifies for the relative inertia against the discharge reaction.

See also Fig. 99 a - b and c - d showing the fully charged active mass under clear and darkfield illumination with globular PbO_2 (a - b) and standard coralloid PbO_2 (c - d). The EOL of such electrodes was shifted to ~25 cycles as compared to ~10 cycles with an untreated CaSn electrode set, but nevertheless far below the ~85 cycles of a regular CaSn electrode.

(d) The evaluation of an improved curing technique other than the low temperature curing technique

On the basis of the experience we acquired from the preceding tests and the observed failure mechanism, i.e. loss of contact between active mass and grid, the use of an improved curing technique was considered of immediate benefit. The survey of existing CaSn positive electrodes revealed that the expanded metal positives produced by DELCO-REMY showed a particularly good bond between the active mass and the grid in the cured conditions. Therefore, in

collaboration with the DELCO-REMY BATTERY DIVISION in Anderson (Indiana, U.S.A.), several sets of electrodes were prepared with improved active mass adhesion.

In order to eliminate grid configuration conversion problems, the grids were made of the same cast CaSn grids fabricated by SONNENSCHEIN (Germany) as used throughout our study, but pasted and cured by DELCO-GM according to their proprietary process. This process gave an excellent active mass adhesion and no shrinkage fractures with all the electrodes.

In order to be treated under strictly comparable conditions, the two different sets of electrodes had the same amount of cured mass per electrode, i.e. 20 g, and were submitted to the same formation and cycling schedule as similarly tested Battelle electrodes. The results presented in Fig. 100 show the relative evolution of the capacities. Whereas with the Battelle and other industrially prepared electrodes, practically all the CaSn batches showed one or more electrodes with an early failure, i.e. a Sb^{II} effect, the equivalent DELCO prepared electrodes showed no such early failures.

This can be attributed to:

(a) the absence of shrinkage fractures;

(b) a rigid active mass due to $4PbO \cdot PbSO_4$ crystals, and

(c) to the cured mass's excellent adhesion to the grid.

We consider that factor (c), good adhesion and (a), absence of shrinkage fractures, were the key elements for a consistently failure-free CaSn electrode production with this method.
This should be considered as a very important achievement for a maintenance-free CaSn traction battery.

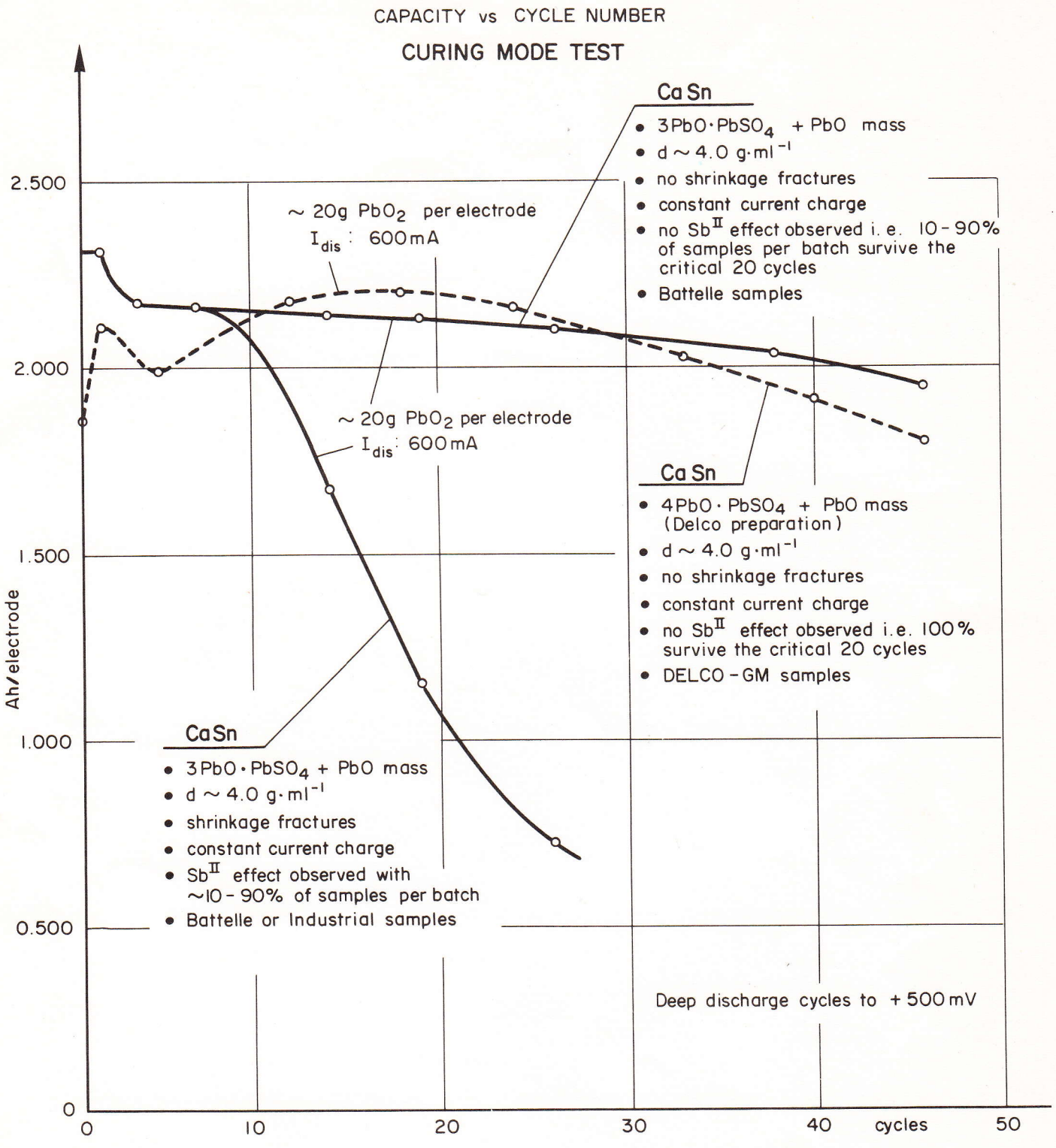

Fig. 100 Influence of the curing technique on the appearance of the Sb^{II} - early failure effect.

A further curing related factor influencing the appearance of the Sb^{II} effect and the relative proportion of early failures was the degree of aging of the mill oxide.

In fact, in our 12 electrode preparation batches, we observed a gradual increase of the early failure proportion, starting with Batch 1 (fresh oxide): 2 failures out of 12 and reaching 10 failures out of 12 with Batch 12 - 8 months later (aged oxide). The utilization of a fresh oxide batch again brought the failure rate down as with Batch 13 (fresh oxide): 1 failure out of 12 electrodes.

Analyis revealed that the free Pb content fell from ~30% to 18%, together with a decrease of apparent density of the oxide powder from ~2.1 to 1.97 $g \cdot ml^{-1}$.

The relative aging of the ball mill oxide and the connected appearance of increased shrinkage fractures appear to be important factors.The absolute free Pb content is not critical, as the Barton oxide batch with 9% free Pb - freshly prepared - gave a very satisfactory behaviour with minimal early failures. We presume that the water binding properties, given by the reactivity of the free Pb, are impaired and result in an increased shrinking tendency of the cured mass.

(e) Influence of charge mode on the Sb^{II} effect

One of the key factors modifying the interface grid-active mass is the growth of the cycling corrosion layer. Its compactness influences both electrical conductivity and the degree of its participation in the $PbO_2 \rightarrow PbSO_4$ discharge reaction. Furthermore, the CCL-AM intergrowth assures the vital link between the current "collector" and the current "donor".

From previous research and discussion with U.S. and European sponsors, the importance of the electrode potential on the nature and structure of the corrosion product was realized. A logical step in the selection of the corrosion product and its growth rate was therefore to limit the electrode potential attained during charge as carried out in practice with the constant voltage charge mode.

Comparative tests were carried out with the following sample sets:

- 4 CaSn electrodes with shrinkage fractures. These were replicates of a set which gave a 100% failure rate after 20 cycles under constant current charging;
- 12 replicates of CaSn electrodes without shrinkage fractures (fresh ball mill oxide as base for the paste) for constant current charge;
- 16 replicates of CaSn electrodes without shrinkage fractures (fresh ball mill oxide as base for the paste) for constant voltage charge.

Results:

The charge and discharge rate conditions of the cycled electrodes were executed under as similar conditions as possible .

The potential reached at the end of discharge was substantially identical, i.e. +500 mV positive electrode potential (vs Hg/Hg_2SO_4). This was achieved in one case by setting this value as the limit for the discharge (constant current test CCT), and in the other case (constant voltage test CVT) by setting 1560 mV cell voltage as the discharge limit. Both electrode sets therefore reached a similar end-of-discharge potential.

During charge, the rate with which ~85 - 90% of the extracted capacity was re-introduced was again similar. This was achieved by a maximum current limit in the CVT of the same value as the constant current value in the CCT, i.e. 500 or 600 mA.

The main difference resulting from this charging practice concerned:

the overcharge, i.e. the excess ampere hours introduced::

20% in the CC test
4 - 9% in the CV test;

the electrode potential reached:

CCT : ~+1450 mV vs Hg/Hg_2SO_4
CVT : shortly +1420 mV, principally +1350 mV;

and the period above a certain potential:

CCT : ~300 mn above +1400 mV with a failing electrode
~60 - 180 mn above +1400 mV with a normal electrode,

CVT : ~20 mn above +1400 mV in all cases.

Since the corrosion of the CaSn electrode rises rapidly between +1400 mV and +1500 mV, we suppose that this increased corrosion weakens the already damaged interface by modifying it in such a way to induce early failures. Previous tests showed a 30-fold rise in corrosion between +1400 mV and +1500 mV and a 100-fold rise between +1500 mV and +1600 mV. We recall that Sb electrodes corrode proportionally much faster (by a factor ~10) than the CaSn electrodes, but the presence of Sb seems to allow a continuous good contact with the active mass.

92a

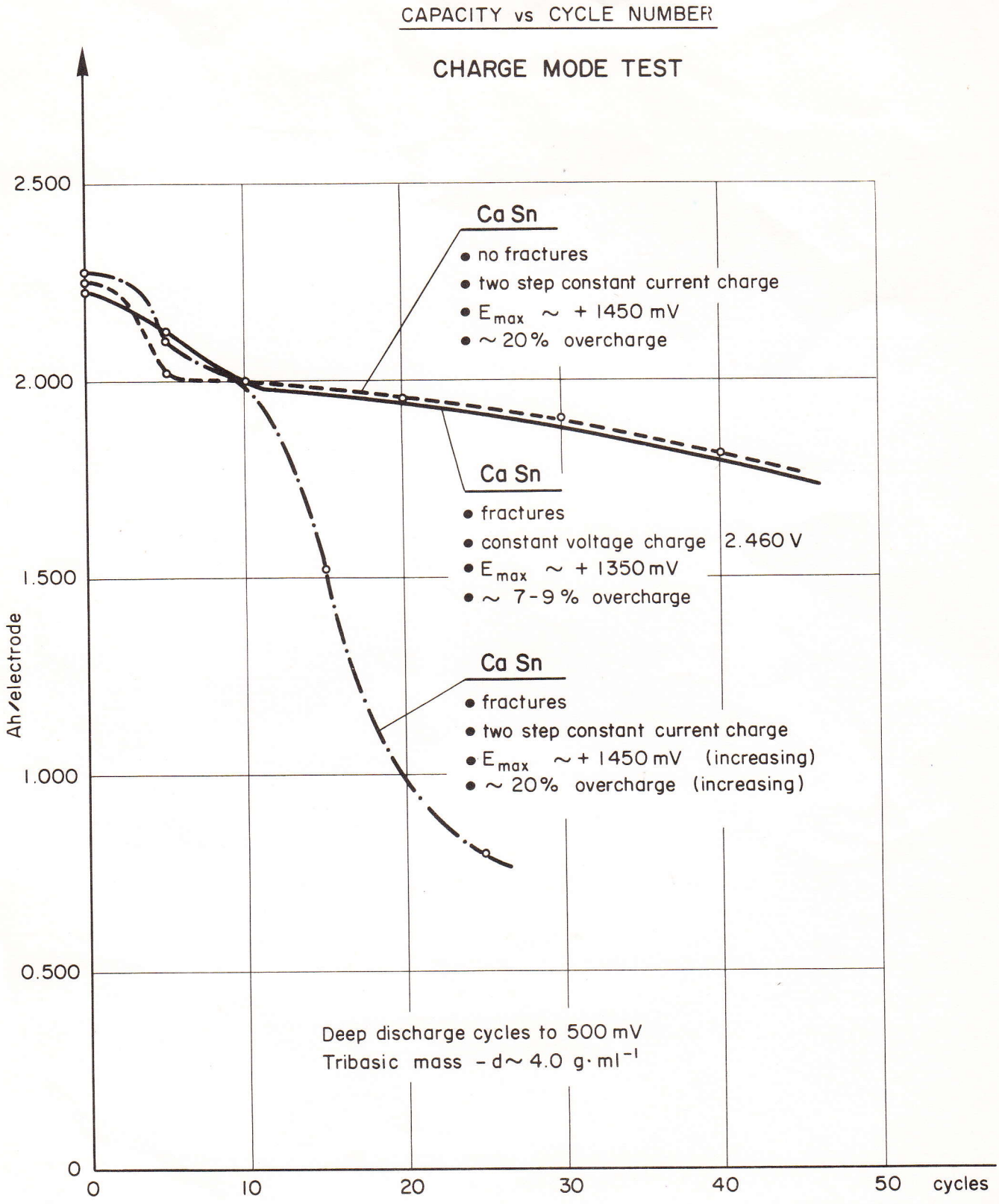

Fig. 101 Influence of the charging mode on the appearance of the Sb^{II} - early failure effect.

As Fig. 101 shows, we observe

- zero failure in the CVT with the set of damaged electrodes where with sister samples a 100% failure rate was observed;
- zero failure in CVT with the set of electrodes where the equivalent samples showed 3 failures out of 24 electrodes.

The current limited constant voltage charge would therefore seem to successfully eliminate the early failures - Sb^{II} effect, by reducing the damage caused by increased corrosion.

The limits for the application of such a charging type reside in the possibility of keeping the positive electrode potential at ~+1350 mV to +1370 mV at 25°C for most of the charging period. Note that the imposition of the cell voltage of 2,460 V does not automatically guarantee such potential as this very much depends on the dimension of the negative electrode. In fact, this negative electrode, polarizing very strongly towards the end of charge, depresses the current flow through the cell, hence, the polarization and potential of the positive electrode.

We suggest that the positive electrode potential limit of ~+1350 mV vs Hg/Hg_2SO_4 in 1.285 sp.gr. H_2SO_4 should be explored individually by the sponsor companies in order to adjust this potential limit to their electrode quality.

Conclusions concerning the Sb^{II} - early failure - effect

The random early failures during deep cycling of CaSn electrodes are ascribed to the destruction of adequate electronic contact between the grid-CCL and the active mass.

This unfavourable interface status already exists during curing and is accentuated by the unfavourable evolution toward fine and low strength crystal agglomerates of the structure of the PbO_2 producing the CCL-AM bond.

The early failures can be most conveniently prevented by:

(a) adequate curing techniques, and
(b) mild constant voltage charging.

The artificial addition of antimony into the positive electrode system also prevents the appearance of such failures under certain circumstances, but the basic advantages of the CaSn grid, i.e. the maintenance-free effect, is impaired.

3.5.3. LOW DENSITY ACTIVE MASS STRUCTURES WITH Sb-FREE GRIDS - LODEF EFFECT

In the course of our investigations of low density active masses with good adhesion properties to the grid, we observed an accelerated capacity decay in terms of the relative cycle number reached with CaSn electrodes before EOL. This accelerated capacity decay was observed with CaSn grids pasted with a $4PbO \cdot PbSO_4$ + PbO mass with a density of 3.37 $g \cdot ml^{-1}$ and 3.07 $g \cdot ml^{-1}$ after curing. These sets of electrodes in the chapter on "Electrode Preparation", are denominated DELCO-1 and DELCO-2 respectively.

As this accelerated capacity decay was very reproducible and not, as the previously discussed Sb^{II} effect, i.e. early failures, random, nor traceable to defects in the electrode, an extensive investigation of this effect was undertaken.

FLOW SHEET OF THE Sb^{II} - EARLY FAILURE - EFFECT

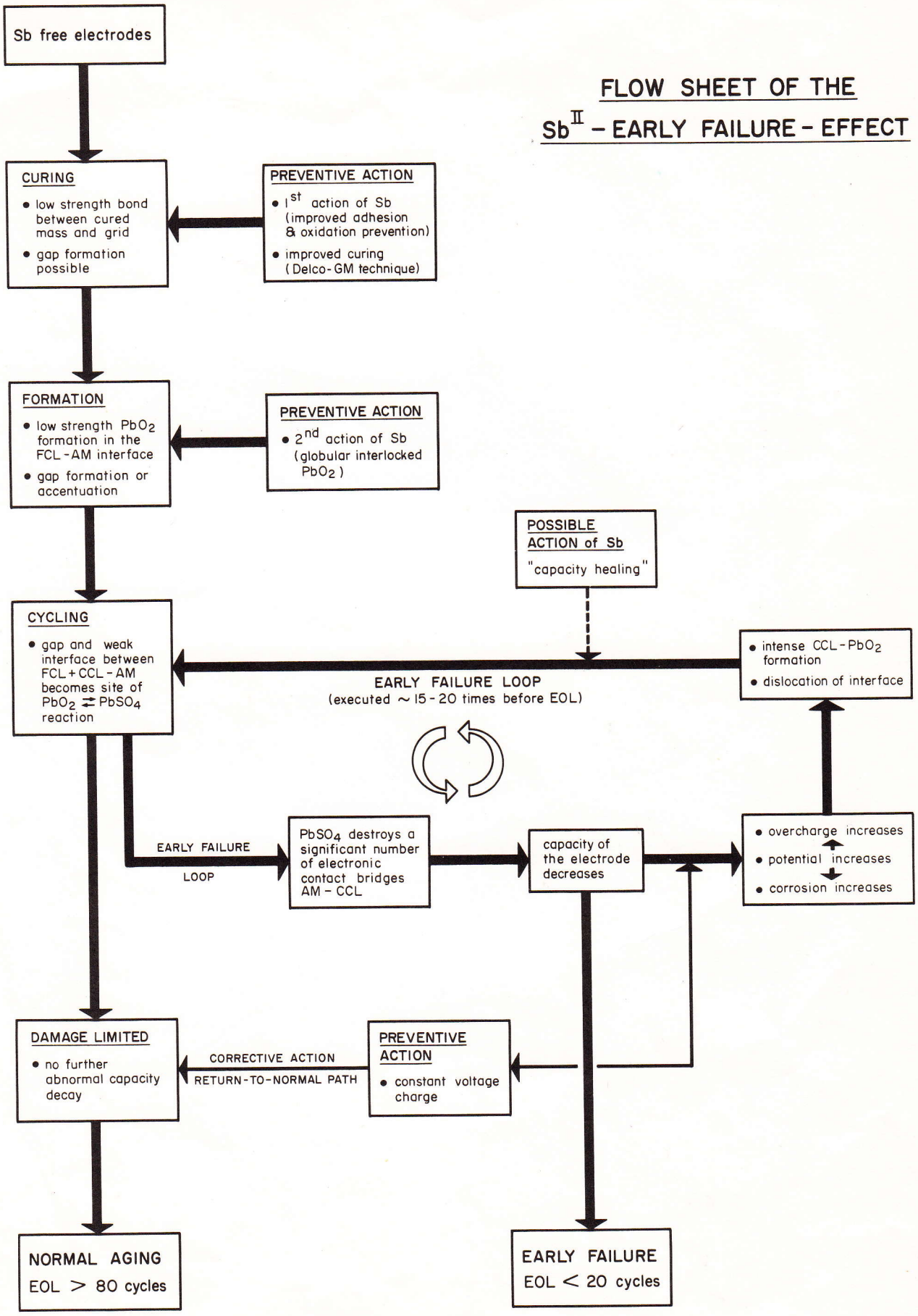

Results

The experiments were again based on comparative tests with 7 Sb grid electrodes acting as the reference point. The electrodes employed were prepared in three distinct preparations by DELCO-GM (U.S.A.) and were based on the same high temperature-cured mass system. The key variable was the relative active mass density and the resulting quantity of paste on the grid.

The values shown in Table 25 were:

TABLE 25

DELCO-1	- 3.39 $g \cdot ml^{-1}$ dry density before formation - 17.5 g cured mass·electrode
DELCO-2	- 3.07 $g \cdot ml^{-1}$ dry density before formation - 15.7 g cured mass·electrode
DELCO-3	- 3.78 $g \cdot ml^{-1}$ dry density before formation - ~20.3 g cured mass·electrode

The sets DELCO-2 and -3 also contained long Dynel-type fibres.

The capacity vs cycle number curves are shown in Fig. 102 for the three electrode sets.

The basic results obtained from these experiments were:

- the increase of density of the mass from ~3.07 - 3.39 to 3.78 $g \cdot ml^{-1}$ doubles the number of cycles before EOL with 7 Sb alloy grids and approximately quadruples the life in terms of cycles of CaSn alloy grids:

- the shedding of the low density mass electrodes is variable and not suitable as an indicator of failure.

  ~45 cycles
  EOL DELCO-1 7 Sb ~4.7 g shedded
  EOL DELCO-2 7 Sb ~1.3 g shedded

  ~22 cycles
  EOL DELCO-1 CaSn ~3.0 g shedded
  EOL DELCO-2 CaSn ~0.6 g shedded;

- the difference in capacity decay of low and high density paste CaSn electrodes is remarkable.

  With "low" density paste this amounts to ~0.16 - 0.2 Ah·cycle^{-1} with CaSn grids, and only to ~0.05 Ah·cycle^{-1} with 7 Sb grids (CaSn/7 Sb K = 3.2 - 4.0).

  With "high" density paste the difference under comparable conditions is very small with both electrode types, showing ~0.01 - 0.03 Ah·cycle^{-1} (CaSn/7 Sb K = 1.0).

This indicates that at low active mass densities, a second and new life limiting factor is at work.

We will therefore now present the additional investigations according to the following schedule:

- comparative failure analysis;
- selected modification of d.o.d.;
- influence of phosphoric acid additions;

and conclude with the overall discussion of these effects on the Sb-free electrodes.

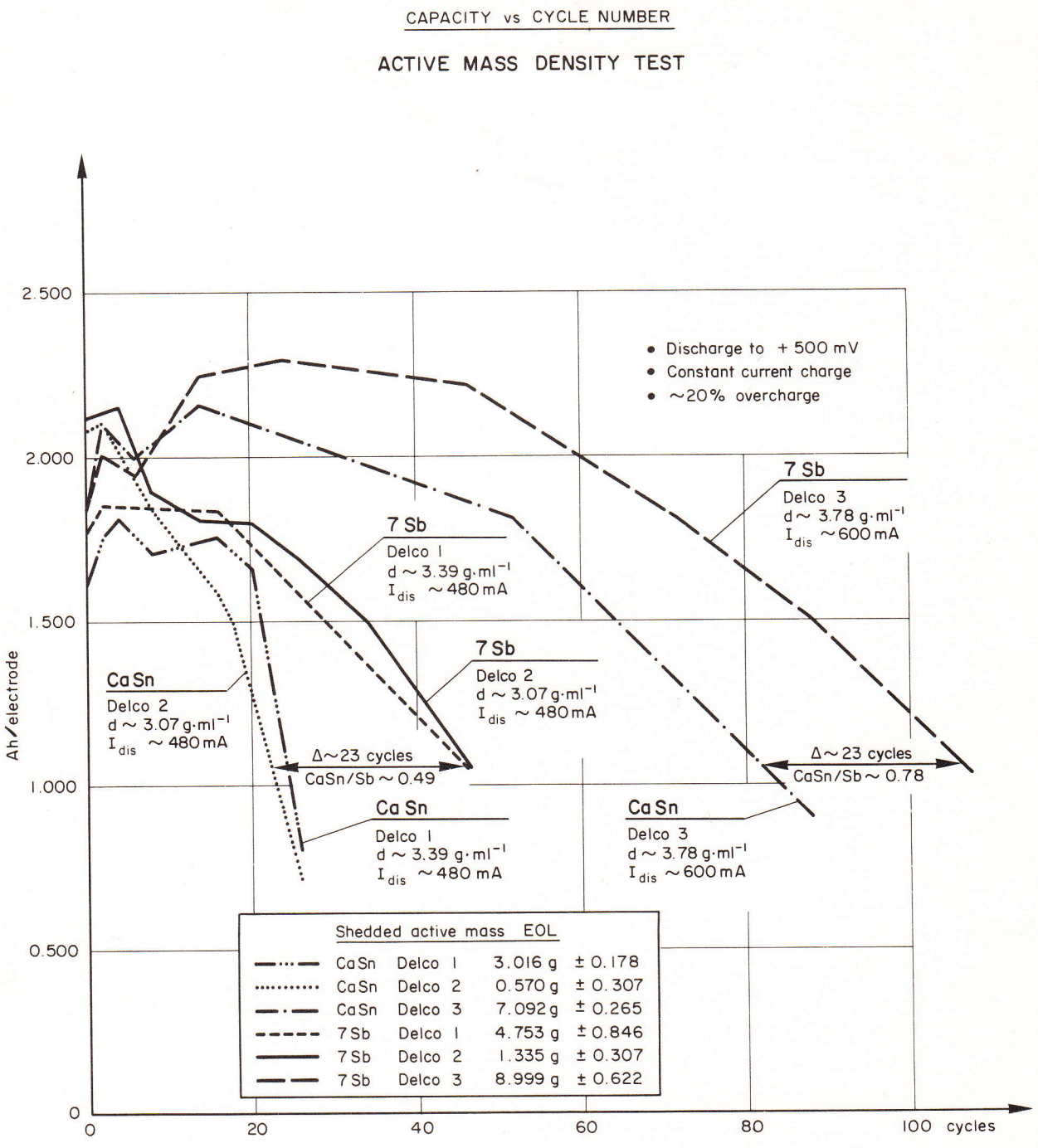

Fig. 102 Evolution of the electrode capacity in function of the apparent active mass density.